NASA CONTRACTOR REPORT **NASA CR-111921**

CALCULATION OF INVISCID SURFACE STREAMLINES AND HEAT TRANSFER ON SHUTTLE TYPE CONFIGURATIONS

Part I. - Description of Basic Method

by Fred R. DeJarnette

Prepared by

MECHANICAL AND AEROSPACE ENGINEERING DEPT.
NORTH CAROLINA STATE UNIVERSITY
RALEIGH, NORTH CAROLINA 27607

for

LANGLEY RESEARCH CENTER
NATIONAL AERONAUTICS AND SPACE ADMINISTRATION
HAMPTON, VIRGINIA 23365

AUGUST, 1971

NASA CR-111921

CALCULATION OF INVISCID SURFACE STREAMLINES AND HEAT TRANSFER ON SHUTTLE TYPE CONFIGURATIONS

Part I. - Description of Basic Method

by Fred R. DeJarnette

Prepared under Contract No. NAS1-10277 by
Mechanical and Aerospace Engineering Dept.
NORTH CAROLINA STATE UNIVERSITY
Raleigh, North Carolina

for Langley Research Center

NATIONAL AERONAUTICS AND SPACE ADMINISTRATION

For sale by the Clearinghouse for Federal Scientific and Technical Information
Springfield, Virginia 22151 - CFSTI price $3.00

PRECEDING PAGE BLANK NOT FILMED

FOREWORD

This research was supported under contract NAS1-10277 with the National Aeronautics and Space Administration's Langley Research Center. The technical monitor on the contract was H. Harris Hamilton II. The results are published in two parts:

Part I Description of Basic Method (NASA CR 111921)

Part II Description of Computer Program (NASA CR 111922)

Part I contains a detailed description of the theoretical approach and basic equations that were used to obtain a solution to the problem. Part II contains a detailed description of the computer program and is intended to serve primarily as a users' manual.

ACKNOWLEDGMENTS

The author would like to express his appreciation to Mr. H. Harris Hamilton, II of the Langley Research Center, NASA for his review of the manuscript and valuable assistance during all phases of this work. In addition, the helpful discussions of Mr. James C. Dunavant of the Langley Research Center, NASA are gratefully acknowledged.

The author would also like to thank the following people at the North Carolina State University:

1. Mr. Michael H. Jones for his assistance in the development of the computer program and preparation of figures for this report.
2. Mrs. Joyce Sorensen for typing the manuscript and assisting with the printing.
3. Miss Eleanor Bridgers for her assistance in the printing and assembling of this report.

PRECEDING PAGE BLANK NOT FILMED

CONTENTS

CALCULATION OF INVISCID SURFACE STREAMLINES AND HEAT TRANSFER ON SHUTTLE TYPE CONFIGURATIONS

Part I - Description of Basic Method

By Fred R. DeJarnette
North Carolina State University

SUMMARY

A computer program is developed which calculates laminar, transitional, and turbulent heating rates on arbitrary blunt-nosed three-dimensional bodies at an angle of attack in hypersonic flows. The geometry of the body is generated from a two-dimensional cubic spline fit to coordinates at several axial stations along the body. Inviscid surface streamlines are calculated optionally from input pressure distributions or modified Newtonian pressures. Laminar and turbulent heating rates are determined along a streamline from the application of the axisymmetric analogue, or small cross flow assumption. The transition region is specified optionally by geometric location, momentum thickness Reynolds number, or integrated unit Reynolds number along a streamline. Transition heating rates are then calculated as a weighted average of the local laminar and turbulent values. Either perfect gas or equilibrium air properties may be specified.

Results are presented for a blunted 15° half-angle cone, a blunted 70° delta wing, and the HL-10 lifting body. By comparison with experimental data for the blunted cone the method was found to yield reasonably accurate laminar heating rates for this case.

INTRODUCTION

Space shuttle vehicles are subjected to severe aerodynamic heating during the reentry phase of their trajectories. In order to design appropriate thermal protection systems, the heat-transfer rates to the exposed surfaces are required. Since many different configurations and flight conditions are being considered for the space shuttle, existing experimental heating rates are insufficient, and an exhaustive new experimental program would be very costly. This part of the report presents an analytical method for calculating laminar, transitional, and turbulent heating rates on general three-dimensional bodies for a wide range of reentry flight conditions. A description of the computer program appears in Part II (NASA CR 111922).

For those flight conditions where aerodynamic heating is important, the flow field generally can be represented by a boundary layer adjacent to the surface and an inviscid layer between the boundary layer and bow shock wave. Reentry velocities are high enough to cause the gas in the shock layer to deviate from a perfect gas, but sufficiently low (less than 30,000 ft/sec) that radiative heat transfer is small compared to convective heating.

Numerical methods are currently available for calculating inviscid and boundary-layer flow-fields over two-dimensional and axisymmetric bodies at zero angle-of-attack (e.g. refs. 1 and 2). Also, methods for calculating inviscid flow fields over pointed and spherically blunted three-dimensional bodies have been developed (e.g. refs. 3 and 4). However, these techniques require considerable storage and computational time on existing digital computers, and a satisfactory three-dimensional boundary-layer program is not available. The problem is further complicated by the fact that shuttle type configurations are general three-dimensional bodies whose geometry is difficult to describe analytically. During reentry they operate at large angles of attack, and laminar, transitional, and turbulent heating may occur.

If tractable solutions of three-dimensional flow fields are to be obtained, simplifying approximations must be used for the inviscid and viscous flow-fields. A substantial simplification to the viscous flow field may be achieved by the axisymmetric analogue, or small cross flow approximation, for three-dimensional boundary layers (refs. 5 and 6). This approximation allows the heat transfer rate along a surface inviscid streamline to be calculated by any method applicable to an equivalent body of revolution at zero angle-of-attack provided the surface inviscid solution is known. Along each streamline the "equivalent radius" or scale factor replaces the radius of the body of revolution in the axisymmetric analogue, and the distance along a streamline replaces distance along the body of revolution. Thus each surface inviscid streamline on the three-dimensional body corresponds to a different equivalent body of revolution at zero angle-of-attack.

In order to apply the axisymmetric analogue, the inviscid solution at the edge of the boundary layer must be known. For blunt nosed bodies with thin boundary layers, the flow field properties at the edge of the boundary layer are nearly the same as the corresponding inviscid solution on the surface. If the surface streamlines are assumed to pass through the normal part of the bow shock wave, then the surface entropy (for a perfect or equilibrium gas) is equal to the entropy aft of the normal shock wave.[+] The remaining inviscid solution needed for the boundary layer solution can be calculated from the pressure distribution; and when the pressure distribution is unknown, modified Newtonian pressures can be used.

One of the major difficulties in applying the axisymmetric analogue is the calculation of the surface inviscid streamlines and the corresponding "equivalent radius" or scale factor. References 7, 8, and 9 present several approaches for calculating the surface inviscid streamlines. Approximate methods for determining the "equivalent radius" are given by Timmer (ref. 9), Pinkus and Cousin (ref. 10) and Vaglio-Laurin (ref. 11), whereas references 12 and 13 determined equivalent radii on blunted cones at an angle of attack by calculating the spacing between streamlines. These approximate techniques are not satisfactory for general three-dimensional bodies.

DeJarnette and Davis (ref. 14) determined an analytical expression for the "equivalent radius" on blunted cones at an angle of attack based on a simplified method for calculating the streamlines.[*] Later DeJarnette and Tai (ref. 15) developed an "exact" method for calculating the streamlines and "equivalent radius" from surface pressure distributions on axisymmetric bodies at an angle of attack. Both techniques are extended to general three-dimensional bodies in this report.

+ This assumption is invalid in those regions where the boundary layer has "swallowed" the entropy layer.

* DeJarnette also obtained analytical results for elliptic cones at an angle of attack, using this simplified method, while participating in the NASA-ASEE Summer Faculty Research Program at Ames Research Center, NASA, Summer, 1969 (unpublished).

Another difficulty associated with the surface streamlines is their behavior in a three-dimensional stagnation region. The stagnation point is a singular point (nodal point), and thus numerical problems are normally encountered there. These problems are solved in the present method by developing analytical expressions for the streamline geometry and "equivalent radius" in the neighborhood of the stagnation point.

In the application of the axisymmetric analogue along each surface inviscid streamline, methods are required for the calculation of laminar, transitional, and turbulent heating rates on an equivalent body of revolution at zero angle-of-attack. Techniques which involve the numerical solution of the appropriate boundary layer equations, e.g. ref. 2, could be used; however, this approach would destroy the simplicity and short computational time desired in the present method. Therefore, approximate solutions of the boundary layer equations on a body of revolution will be applied.

Lees' method (ref. 16) was used with the axisymmetric analogue to calculate laminar heating rates on blunted cones at an angle of attack in references 14 and 15, and the results compared well with experimental data. However, Lees' method neglects pressure gradient effects and is valid only for cold walls. As a better approximation, the present method uses the local similarity method of Beckwith and Cohen (ref. 17), which includes the effects of pressure gradients and non-cold walls on laminar heating rates. However, special consideration must be given to the application of this method to three-dimensional stagnation points.

The analytical calculation of transitional heating rates and location of the transition region has been unsuccessful to date, and the reader is referred to ref. 2 for a discussion of this phenomenon. For the present work, transitional heating rates are computed as a weighted sum of the laminar and turbulent heating rates, using the weighting distribution of Dhawan and Narasimha (ref. 18). Along a surface inviscid streamline, the beginning and end of transition may be specified optionally by one of the following three parameters:

1. geometric location, or
2. value of local momentum thickness Reynolds number, or
3. value of integrated unit Reynolds number along a streamline.

Many methods have been developed for calculating turbulent boundary layer properties (see discussion in ref. 2). As a compromise between accuracy and simplicity, the technique developed by Spalding and Chi (ref. 19) for calculating turbulent skin friction coefficients based on momentum thickness Reynolds number is used here. The momentum thickness is calculated from the integral method of Reshotko and Tucker (ref. 20) for use in Spalding and Chi's equations. Then the skin friction coefficients are converted to turbulent heating rates through von Karman's form of Reynolds analogy (see ref. 21).

For the applications herein, both a perfect gas and equilibrium air are considered. Therefore, modifications to the methods of Spalding and Chi (ref. 19), and Reshotko and Tucker (ref. 20) are needed to make them applicable to equilibrium air. To keep the computations down to a minimum, the correlation formulas of reference 22 are used for equilibrium air properties.

Results from the computer program are presented for a blunted 15° half-angle cone, a blunted 70° delta wing, and the HL-10 lifting body as example applications of the basic method.

SYMBOLS

a, b	parameters defined by eqs. (150) and (151)
a_e	speed of sound at edge of boundary layer, ft/sec
a_j, b_j, c_j, d_j	constants used in eq. (11)
$A_{i,k}$	coefficients for spline function defined by eq. (25)
B	Ratio of principal velocity gradients, see eq. (107)
$B_{i,k}$	coefficients for spline function defined by eq. (25)
$C(\beta)$	parameter used in eq. (95)
C_f	local skin friction coefficient, $2\tau_w/(\rho_e U_e^2)$
$C_{f,i}$	incompressible skin friction coefficient
D/DS	derivative along a streamline
$\hat{e}_{NN}, \hat{e}_T, \hat{e}_{11}$	unit vectors on body surface given by eqs. (33), (35), and (36)

$\hat{e}_s, \hat{e}_n, \hat{e}_\beta$	unit vectors in streamline coordinate system, eqs. (37), (34), and (38)
$\hat{e}_x, \hat{e}_r, \hat{e}_\phi$	unit vectors in cylindrical coordinate system, see fig. 3
$e(\phi)$	eccentricity of conic section
f	body radius, measured from longitudinal axis
f_Δ	cubic spline function for body radius
F_c	function defined by eq. (177)
$F_{R\delta}$	function defined by eq. (171)
g	function defined by eq. (29)
h	scale factor in β-direction, $dq = h\ d\beta$
h_{aw}	adiabatic wall enthalpy, ft^2/sec^2
h_{bl}, h_e	enthalpy inside and at edge of boundary layer, respectively, ft^2/sec^2
h_w	wall enthalpy, ft^2/sec^2
h_E	reference enthalpy, $2.119 \times 10^8\ ft^2/sec^2$
h_s	scale factor in s-direction, $ds = h_s d\xi$
H	compressible form factor, $H = \delta^*/\theta_m$
H_i	incompressible form factor
H_{tr}	transformed form factor
h_2	static enthalpy aft of normal shock, ft^2/sec^2
H_s	free-stream stagnation enthalpy, ft^2/sec^2
m	coefficient used in cubic spline function
M	Mach number
n	straight-line distance normal to body surface
$N_{ST}, N_{ST,i}$	compressible and incompressible Stanton numbers, respectively
p	pressure, lb/ft^2
p_j, q_j, u_j	parameters defined by eq. (12)

Pr	Prandtl number
q	distance normal to streamline on body surface, $dq = h\, d\beta$
q_w	heat-transfer rate at wall, BTU/ft^2-sec
r	body radius ($r = f$)
$R_o(\phi)$	body radius of curvature at nose
R_T, R_{11}	principal body radii of curvature at stagnation point
R_δ, Rn_m	momentum thickness Reynolds number
Rn_1	integrated unit Reynolds number, $\int_0^s \frac{\rho_e U_e dS}{\mu_e}$
$\bar{R}$	gas constant for undissociated air, 1716 ft^2/sec^2-°R
$\vec{R}$	position vector for points on body
S	distance along a streamline, measured from stagnation point ($dS = h_s d\xi$)
S_{11}, S_T	body coordinates at stagnation point
$\bar{S}$	entropy
t	time, sec
t_e	enthalpy ratio, h_e/H_s
T	temperature, °R
U, U_e	velocity inside and at edge of boundary layer, respectively, ft/sec
U_G^+	function defined by eq. (174)
v_2	velocity aft of normal shock wave, ft/sec
V	inviscid speed on surface, ft/sec
$\vec{V}$	inviscid velocity on surface, ft/sec
V_{11}, V_T	velocity components along S_{11} and S_T, ft/sec
$\hat{V}_\infty$	unit vector in direction of freestream velocity vector
w_f	weighting function given by eq. (161)
x, y, z	Cartesian coordinates

α	angle of attack
β	coordinate normal to streamline on body surface
$\overline{\beta}$	pressure gradient parameter given by eq. (146)
γ	ratio of specific heats
Γ	body angle defined by eq. (30)
δ^*	displacement thickness
δ_ϕ	body angle defined by eq. (31)
ϵ	radius of circle around stagnation point, see fig. 6
ζ_w	wall enthalpy ratio, h_w/H_s
ζ_w'	enthalpy gradient normal to wall
θ	inclination angle of surface inviscid streamline, see eq. (37)
ϑ_m	momentum thickness, ft
λ	parameter defined by eq. (163)
μ	coefficient of viscosity, slug/ft-sec
ξ	coordinate along a streamline ($dS = h_s d\xi$)
ξ_{tr}	parameter defined by eq. (162)
ρ	mass density, slug/ft^3
σ	angle defined by eq. (47)
τ_w	wall shear stress, lb/ft^2
ϕ	circumferential angle, see fig. 4
ψ	angle defined by eq. (78)

Subscripts:

e	edge of boundary layer
lam	laminar value
s	stagnation point

turb	turbulent value
w	evaluated at wall
ε	evaluated on ε-circle, (see fig. 6)
∞	freestream conditions
tre	end of transition region
tri	beginning of transition region
2	conditions aft of normal shock wave

ANALYSIS

Geometry for General Three-Dimensional Bodies

Before heating rates can be calculated, a description of the body geometry is needed which yields slopes and radii of curvature in both the axial and circumferential directions. If the body could be described by analytic equations, these results would be easily obtainable. However, the geometry of shuttle-type configurations cannot, in general, be represented by an analytic equation. Often only the coordinates of the body at several axial stations are known, and the body geometry must be generated from this data. Therefore, a numerical method is required to generate the body shape and calculate slopes and radii of curvature at any position on the body. This method must be capable of performing numerical interpolation and differentiation reasonably accurately.

It is well known that numerical differentiation is generally inaccurate. However, the method of splines (see ref. 23) has been proven to be an affective method for numerical differentiation, integration, and interpolation. The effectiveness of the cubic spline to perform these operations accurately is a consequence of the strong convergence properties it possesses. Before discussing the two-dimensional cubic spline, which is needed to describe a three-dimensional body, the one-dimensional spline will be developed first.

To illustrate the cubic spline for one dimension (one independent variable), consider the coordinates of a body cross-section (viewed from the rear) with one plane of symmetry as shown in figure 1.

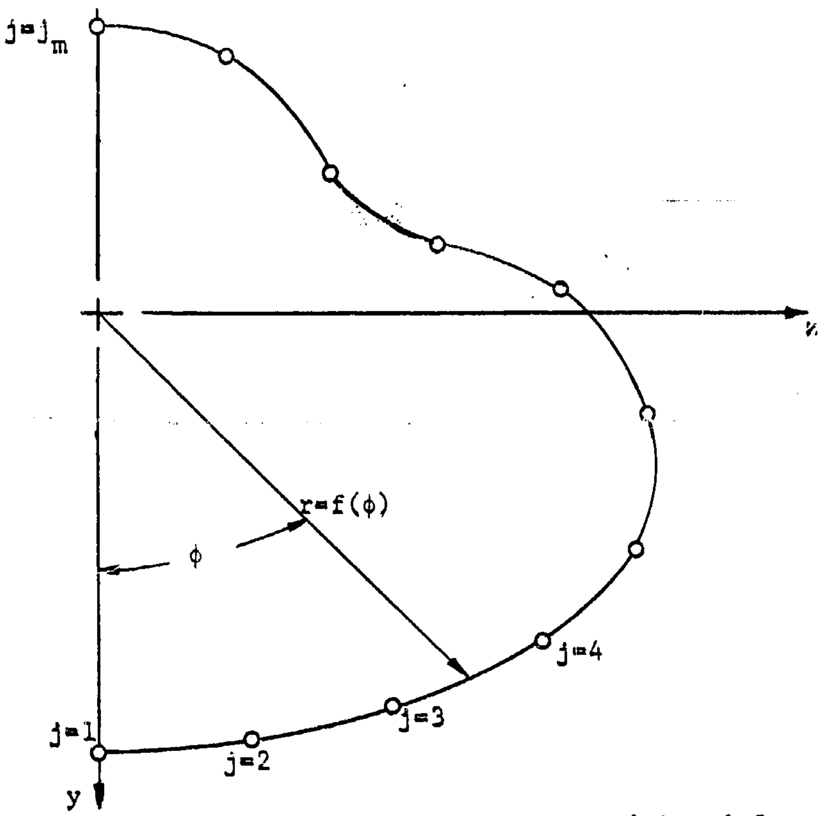

Figure 1. - Coordinates of body cross section (viewed from rear)

For the interval $0 \le \phi \le \pi$, a mesh Δ of body positions is given by (y_j, z_j) with $j = 1, 2, \ldots, j_m$. It is convenient to transform these coordinates into polar coordinates by the transformation

$$r_j \equiv f_j = [y_j^2 + z_j^2]^{1/2} \qquad (1)$$

$$\phi_j = \tan^{-1}(z_j/y_j) \qquad (2)$$

where

$$0 = \phi_1 < \phi_2 < \ldots < \phi_{j_m} = \pi$$

and ϕ is the independent variable. Then the cubic spline for this mesh yields a function $f_\Delta(\phi)$ which is (1) continuous with its first and second derivatives on $[0, \pi]$, (2) coincides with a cubic in each subinterval $\phi_{j-1} \le \phi \le \phi_j$ ($j = 2, 3, \ldots, j_m$), and (3) satisfies $f_\Delta(\phi_j) = f_j$ ($j = 1, 2, \ldots, j_m$). Note that the points $\phi_1, \phi_2, \ldots, \phi_{j_m}$ need not be equally spaced.

Denoting $f_\Delta''(\phi_j) = \frac{d^2 f_\Delta(\phi_j)}{d\phi^2}$ by m_j, the cubic spline on the subinterval $[\phi_{j-1}, \phi_j]$ is assumed to have a linear variation of the second derivative, i.e.

$$f_\Delta''(\phi) = m_{j-1} \frac{(\phi_j - \phi)}{\Delta\phi_j} + m_j \frac{(\phi - \phi_{j-1})}{\Delta\phi_j} \tag{3}$$

where $\Delta\phi_j = \phi_j - \phi_{j-1}$. Then by integrating the above expression and evaluating the constants of integration, the first derivative and spline functions on $[\phi_{j-1}, \phi_j]$ are

$$f_\Delta'(\phi) = -m_{j-1} \frac{(\phi_j - \phi)^2}{2\,\Delta\phi_j} + m_j \frac{(\phi - \phi_{j-1})^2}{2\,\Delta\phi_j} + \frac{(f_j - f_{j-1})}{\Delta\phi_j} - (m_j - m_{j-1}) \frac{\Delta\phi_j}{6} \tag{4}$$

and

$$f_\Delta(\phi) = m_{j-1} \frac{(\phi_j - \phi)^3}{6\,\Delta\phi_j} + m_j \frac{(\phi - \phi_{j-1})^3}{6\,\Delta\phi_j} + \left[f_{j-1} - \frac{m_{j-1}\,\Delta\phi_j^2}{6}\right]\frac{(\phi_j - \phi)}{\Delta\phi_j}$$

$$+\left[f_j - \frac{m_j\,\Delta\phi_j^2}{6}\right]\frac{(\phi - \phi_{j-1})}{\Delta\phi_j} \tag{5}$$

In order to apply the equations above, it remains to calculate the second derivatives m_j at the mesh points. By virtue of equations (3) and (5), the functions $f_\Delta''(\phi)$ and $f_\Delta(\phi)$ are continuous on $[0, \pi]$. By equating the one-sided limits of the derivatives at each interior mesh point, $f_\Delta'(\phi_j^-) = f_\Delta'(\phi_j^+)$, the function $f_\Delta'(\phi)$ becomes continuous on $[0, \pi]$. These relations yield

$$\frac{\Delta\phi_j}{6} m_{j-1} + (\Delta\phi_j + \Delta\phi_{j+1}) \frac{m_j}{3} + \frac{\Delta\phi_{j+1}\, m_{j+1}}{6} = \frac{f_{j+1} - f_j}{\Delta\phi_{j+1}} - \frac{(f_j - f_{j-1})}{\Delta\phi_j} \tag{6}$$

for $j = 2, 3, \ldots, j_m - 1$.

Equation (6) gives $(j_m - 2)$ simultaneous equations in the j_m unknowns m_1, $m_2, \ldots, m_{j_m}$. Therefore two additional conditions must be specified, the "end conditions", to determine all the m_j's. If the slopes at the end points, $f_\Delta'(0^+)$ and $f_\Delta'(\pi^-)$, are known, the one-sided derivatives from equation (4) provide the relations

$$2m_1 + m_2 = \frac{6}{\Delta\phi_1}\left[\frac{f_2 - f_1}{\Delta\phi_1} - f_\Delta'(0^+)\right] \tag{7}$$

and

$$m_{j_m-1} + 2m_{j_m} = \frac{6}{\Delta\phi_{j_m}}\left[f'_\Delta(\pi^-) + \frac{f_{j_m-1} - f_{j_m}}{\Delta\phi_{j_m}}\right] \tag{8}$$

If the curve shown in fig. 1 is symmetric about the y-axis, then symmetry dictates that $f'(0^+) = f'(\pi^-) = 0$. Sometimes these slopes are not available, and the second derivatives at the ends are assumed constant over the end intervals, i.e.

$$m_1 = m_2 \qquad \text{and} \qquad m_{j_m-1} = m_{j_m} \tag{9}$$

Another type of end condition is that symmetry requirements may dictate that

$$m_1 = 0 \qquad \text{and} \qquad m_{j_m} = 0 \tag{10}$$

No matter which of the three types of end conditions is used, the system of equations given by equation (6) and the end conditions may be written as

$$\left.\begin{aligned}
b_1 m_1 + c_1 m_2 &= d_1 \\
a_2 m_1 + b_2 m_2 + c_2 m_3 &= d_2 \\
a_3 m_2 + b_3 m_3 + c_3 m_4 &= d_3 \\
&\text{---} \\
a_{j_m-1}\, m_{j_m-2} + b_{j_m-1}\, m_{j_m-1} + c_{j_m-1}\, m_{j_m} &= d_{j_m-1} \\
a_{j_m}\, m_{j_m-1} + b_{j_m}\, m_{j_m} &= d_{j_m}
\end{aligned}\right\} \tag{11}$$

where a_j, b_j, c_j, and d_j are constants. This is a system of j_m linear equations for the m_j's, and it is of the tridiagonal matrix form.

A very efficient algorithm for solving this system is given on page 14 of reference 23. In this algorithm, the following parameters are formed (for $j = 1, 2, \ldots, j_m$):

$$\left.\begin{aligned}
p_j &= a_j\, q_{j-1} + b_j \qquad (q_o = 0) \\
q_j &= -c_j/p_j \\
u_j &= (d_j - a_j\, u_{j-1})/p_j \qquad (u_o = 0)
\end{aligned}\right\} \tag{12}$$

Then by successive elimination of $m_1, m_2, \ldots, m_{j_m} - 1$ from the 2nd, 3rd, ..., j_m-th equations of (12), the following equivalent equation system results:

$$\left.\begin{aligned} & m_{j_m} = u_{j_m} \\ & m_j = q_j\, m_{j+1} + u_j \\ & (j = j_m-1,\ j_m-2,\ \ldots,\ 1) \end{aligned}\right\} \qquad (13)$$

These relations yield m_{j_m}, m_{j_m-1}, ..., m_1 successively. Once the m_j's are evaluated, the functions $f_\Delta(\phi)$, $f_\Delta'(\phi)$, and $f_\Delta''(\phi)$ can be easily calculated from equations (5), (4), and (3), respectively, for any value of ϕ in the interval $0 \le \phi \le \pi$.

The three-dimensional bodies considered herein will be described by $r = f(x,\phi)$ where x is distance along the axis from the nose, ϕ is the circumferential position, $\phi = \tan^{-1}(z/y)$, and r is the radius from the axis, $r = \sqrt{y^2+z^2}$. Cylindrical coordinates were chosen over Cartesian coordinates in order to avoid infinite body slopes in the cross-sectional planes. The body shape is generated from the coordinates (y_{ij}, z_{ij}) of cross sections at several axial stations x_1, x_2, ..., x_{i_m} (see fig. 2).

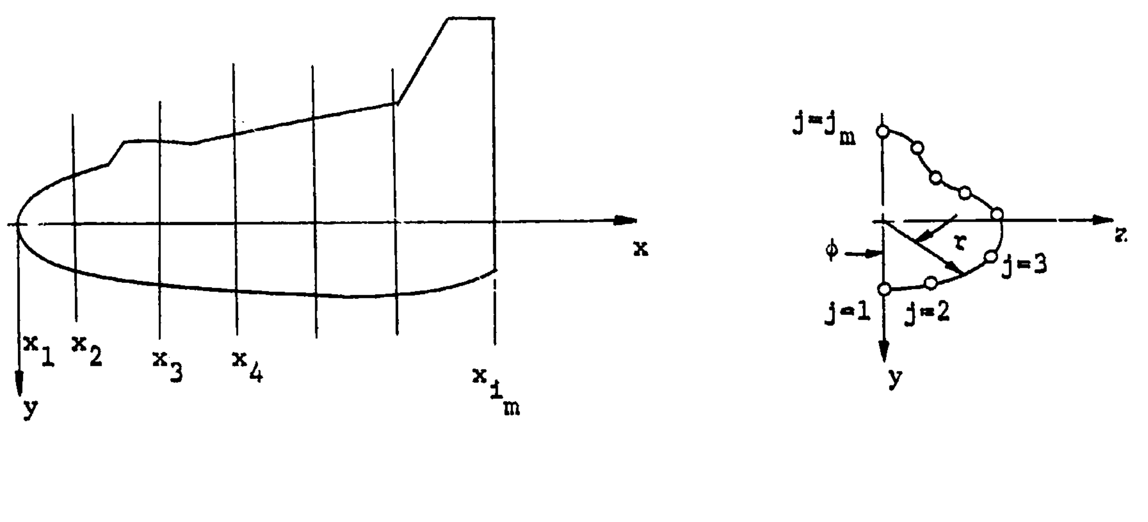

Side view　　　　View from rear

Figure 2. - Body coordinates

Here a two-dimensional spline function is needed to describe the body, and the body shape may be a general three-dimensional body except for the following restrictions:

1. The body must have at least one plane of symmetry.
2. The body radius $r = f(x, \phi)$ must be single valued.
3. The nose of the body must be located at $x = 0$ and at this position $f(0, \phi) = 0$ and $\frac{\partial f}{\partial x}(0, \phi) \to \infty$.

Since the body has at least one plane of symmetry, let this plane be the $x - y$ plane and only the half body $0 \leq \phi \leq \pi$ need be described. A simple doubly cubic spline (see Chapter VII of ref. 23) is used to generate the body shape from the input coordinates. The rectangular region $0 \leq x \leq x_{i_m}$, $0 \leq \phi \leq \pi$ is subdivided into a family of subrectangles $x_{i-1} \leq x \leq x_i$, $\phi_{k-1} \leq \phi \leq \phi_k$ where $0 = x_1 < x_2 < \dots x_{i_m}$ and $0 = \phi_1 < \phi_2 < \dots \phi_{j_m} = \pi$. Thus the simple doubly cubic spline for this two-dimensional mesh yields a function $f_\Delta(x,\phi)$ which is: (1) an element of $C_2^{\,4}(R)$, where $C_r^{\,n}(R)$ is the family of functions $f_\Delta(x,\phi)$ on the rectangular region R whose n-th order partial derivatives, involving no more than r-th order differentiation with respect to a single variable, exist and are continuous; (2) is a double cubic in each subrectangle, and (3) satisfies $f_\Delta(x_i,\phi_k) = f_{ik}$ for each point of the double mesh.

To see how the one-dimensional cubic spline can be extended to the two-dimensional cubic spline, apply the one dimensional spline function $f_\Delta(\phi)$ of equation (5) to each cross section of the body at $x_2, x_3, \dots, x_{i_m}$. If the coordinates ϕ_j are chosen to be the same in each cross section, then the spline function becomes

$$f_\Delta(x_i,\phi) = m_{j-1}(x_i)\,\frac{(\phi_j-\phi)^3}{6\,\Delta\phi_j} + m_j(x_i)\,\frac{(\phi-\phi_{j-1})^3}{6\,\Delta\phi_j} + \left[f_{j-1}(x_i) - \frac{m_{j-1}(x_i)\Delta\phi_j^2}{6}\right]\frac{(\phi_j-\phi)}{\Delta\phi_j} + \left[f_j(x_i) - m_j(x_i)\,\frac{\Delta\phi_j^2}{6}\right]\frac{(\phi-\phi_{j-1})}{\Delta\phi_j} \qquad (14)$$

The quantities which change from one x-station to another are $m_{j-1}(x_i)$, $m_j(x_i)$, $f_{j-1}(x_i)$, and $f_j(x_i)$. Hence, $f_\Delta(x_i,\phi)$ could be applied to any general axial position to yield $f_\Delta(x,\phi)$ if the x-variation of $m_{j-1}(x)$, $m_j(x)$, $f_{j-1}(x)$, and $f_j(x)$ were known. These variations may be determined by forming one-dimensional cubic splines of $m_j(x)$ and $f_j(x)$ from the values of $m_j(x_i)$ and $f_j(x_i)$ at $x = x_1, x_2, \dots, x_{i_m}$ for each value of $j = 1, 2, \dots, j_m$.

The one-dimensional cubic spline function $f_j(x)$ presents an immediate problem because the end condition $\frac{df_j(0)}{dx} \rightarrow \infty$ at the nose cannot be handled. However, for the region $0 = x_1 \leq x \leq x_2$, the axial variation of the radius $r = f(x,\phi)$ for ϕ = constant can be described by a general conic section for most bodies of interest. This general conic section may be written as

$$[f(x,\phi)]^2 = 2R_c(\phi)x + [e^2(\phi) - 1]x^2 \tag{15}$$

where $R_o(\phi)$ is the nose radius of curvature and $e(\phi)$ is the eccentricity of the general conic section ($e = 0$ for a circle, $0 < e < 1$ for an ellipse, $e = 1$ for a parabola, and $e > 1$ for a hyperbola). Therefore, if the function $f^2(x,\phi)$ is used for the doubly cubic spline, in lieu of $f(x,\phi)$, this function is well behaved at $x = 0$, because

$$\frac{\partial f^2(0,\phi)}{\partial x} = 2R_o(\phi) \tag{16}$$

and

$$\frac{\partial^2 f^2(0,\phi)}{\partial x^2} = 2[e^2(\phi) - 1] \tag{17}$$

Thus for the region $0 = x_1 \leq x \leq x_2$ it is seen that

$$\frac{\partial^2 f^2(x,\phi)}{\partial x^2} = 2[e^2(\phi) - 1] \tag{18}$$

which means that

$$\frac{\partial^2 f^2(x_1,\phi)}{\partial x^2} = \frac{\partial^2 f^2(x_2,\phi)}{\partial x^2} \tag{19}$$

and also

$$\frac{\partial^4 f^2(x_1,\phi)}{\partial x^2 \partial \phi^2} = \frac{\partial^4 f^2(x_2,\phi)}{\partial x^2 \partial \phi^2} \tag{20}$$

These two equations are needed for the end conditions below.

In view of the foregoing considerations, the doubly cubic spline representation for $f^2(x,\phi)$ is

$$f_\Delta^2(x,\phi) = m_{k-1}(x)\,\frac{(\phi_k - \phi)^3}{6\,\Delta\phi_k} + m_k(x)\,\frac{(\phi - \phi_{k-1})^3}{6\,\Delta\phi_k}$$

$$+ \left[f_{k-1}^2(x) - m_{k-1}(x)\,\frac{\Delta\phi_k^2}{6}\right]\frac{(\phi_k - \phi)}{k}$$

$$+ \left[f_k^2(x) - m_k(x)\,\frac{\Delta\phi_k^2}{6}\right]\frac{(\phi - \phi_{k-1})}{\Delta\phi_k} \tag{21}$$

where the points $0 = \phi_1 < \phi_2 < \ldots \phi_{k_m}$ are chosen to be equally spaced* around the circumference at each axial station ($\Delta\phi_k = \phi_k - \phi_{k-1}$ = constant). In equation (21)

$$m_k(x) = \frac{\partial^2 f^2(x,\phi_k)}{\partial\phi^2} \tag{22}$$

and $m_k(x)$ and $f_k^2(x)$ are determined from one-dimensional cubic spline fits to the data $m_k(x_i)$ and $f_k^2(x_i)$, respectively, for $i = 1, 2, \ldots, i_m$. For $x_{i-1} \le x \le x_i$ these functions take the form

$$m_k(x) = B_{i-1,k}\,\frac{(x_i - x)^3}{6\,\Delta x_i} + B_{i,k}\,\frac{(x - x_{i-1})^3}{6\,\Delta x_i}$$

$$+ \left[m_{i-1,k} - B_{i-1,k}\,\frac{\Delta x_i^2}{6}\right]\frac{(x_i - x)}{\Delta x_i}$$

$$+ \left[m_{i,k} - B_{i,k}\,\frac{\Delta x_i^2}{6}\right]\frac{(x - x_{i-1})}{\Delta x_i} \tag{23}$$

---

* Although the input body coordinates are not generally equally spaced in the circumferential direction and generally differ from one body cross section to another, a one-dimensional spline fit to the data at each cross section can be used to calculate new points $f_\Delta^2(x_i, \phi_k)$ which are equally spaced in the circumferential direction.

and

$$f_k^2(x) = A_{i-1,k} \frac{(x_i - x)^3}{6\ \Delta x_i} + A_{i,k} \frac{(x - x_{i-1})^3}{6\ \Delta x_i}$$

$$+ [f^2_{i-1,k} - A_{i-1,k} \frac{\Delta x_i^2}{6}] \frac{(x_i - x)}{\Delta x_i}$$

$$+ [f^2_{i,k} - A_{i,k} \frac{\Delta x_i^2}{6}] \frac{(x - x_{i-1})}{\Delta x_i} \tag{24}$$

where

$$\left.\begin{aligned} A_{i,k} &\equiv \frac{\partial^2 f^2}{\partial x^2} (x_i,\phi_k) \\ B_{i,k} &\equiv \frac{\partial^4 f^2}{\partial \phi^2 \partial x^2} (x_i,\phi_k) \\ \Delta x_i &\equiv x_i - x_{i-1} \end{aligned}\right\} \tag{25}$$

The end conditions at $x = 0$ follow from equations (19) and (20) as

$$B_{1,k} = B_{2,k} \qquad \text{and} \qquad A_{1,k} = A_{2,k} \tag{26}$$

In addition, it is assumed that at the end of the body

$$B_{i_m-1,k} = B_{i_m,k} \qquad \text{and} \qquad A_{i_m-1,k} = A_{i_m,k} \tag{27}$$

These last two conditions imply that $\frac{\partial^2 f^2(x,\phi_k)}{\partial \phi^2}$ and $f^2(x,\phi_k)$ have at most a quadratic variation in x over the last subinterval $[x_{i_m-1}, x_{i_m}]$.

In the application of the cubic spline, it should be noted that the spline function passes through every input coordinate point. Therefore, if an input point is incorrect, the spline function still passes through that point. On the other hand, the resulting derivatives from the spline function represent a smoothing of the actual derivatives (see pp. 42-44 of ref. 23). When accurate second derivatives are desired, a spline-fit of the first derivatives (called a spline-on-spline) has been found to be an effective tool.

Inviscid Surface Streamlines

In order to apply the axisymmetric analogue to three-dimensional boundary layers, it is necessary to trace out inviscid surface streamlines and calculate the corresponding "equivalent radius" or scale factor along each streamline. This scale factor (h) is the metric coefficient for the coordinate β normal to the streamline and on the surface of the body. It is a measure of the divergence of the streamlines as they wrap around the body.

An orthogonal coordinate system will be used for the streamline geometry. Let the differential of arc length along a streamline be $dS = h_s\, d\xi$, the differential of arch length normal to a streamline (but on the body surface) be $dq = h\, d\beta$, and the differential of distance normal to the surface be dn. Both h_s and h are metric coefficients or scale factors for the coordinates ξ and β, respectively; however, only the scale factor h is needed for the application of the axisymmetric analogue. Since the coordinate n is the straight-line distance normal to the surface, its scale factor is unity. Along a streamline the coordinate β is constant, but it varies from one streamline to another.

Define the body geometry by Monge's form $r = f(x,\phi)$ in a cylindrical coordinate system with the unit vectors $\hat{e}_x$, $\hat{e}_r$, and $\hat{e}_\phi$ in the x, r, and ϕ directions, respectively (see fig. 3). Note that the cross section at the right of figure 3 is viewed from the rear and that the coordinate system is right handed.

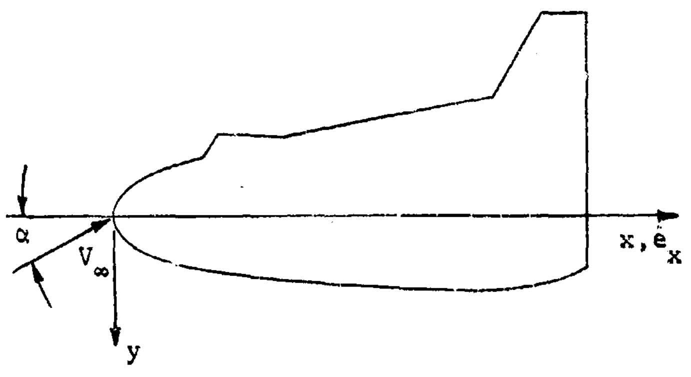

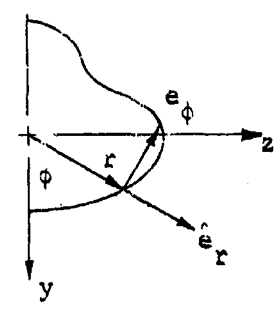

Figure 3. Body Geometry

Define

$$F(x,r,\phi) \equiv r - f(x,\phi) = 0$$

then the unit vector normal (outer) to the surface is

$$\hat{e}_n = \frac{\nabla F}{|\nabla F|} = \frac{-\frac{\partial f}{\partial x}\hat{e}_x + \hat{e}_r - \frac{1}{f}\frac{\partial f}{\partial \phi}\hat{e}_\phi}{g^{1/2}} \tag{28}$$

where

$$g \equiv \left(\frac{\partial f}{\partial x}\right)^2 + 1 + \left[\frac{1}{f}\frac{\partial f}{\partial \phi}\right]^2 \tag{29}$$

Define the body angle $\Gamma(x,\phi)$ by

$$\sin\Gamma = \frac{\frac{\partial f}{\partial x}}{g^{1/2}} \tag{30}$$

where $-\pi/2 \leq \Gamma \leq \pi/2$ and also the body angle $\delta_\phi(x,\phi)$ by

$$\sin\delta_\phi = \frac{\frac{1}{f}\frac{\partial f}{\partial \phi}}{\left[1 + \left(\frac{1}{f}\frac{\partial f}{\partial \phi}\right)^2\right]^{1/2}} \tag{31}$$

where $-\pi/2 \leq \delta_\phi \leq \pi/2$* (see fig. 4). From eqs. (30) and (31) it also follows that

$$\cos\Gamma = \frac{1}{\cos\delta_\phi\, g^{1/2}}$$

and

$$\cos\delta_\phi = \frac{1}{\left[1 + \left(\frac{1}{f}\frac{\partial f}{\partial \phi}\right)^2\right]^{1/2}}$$

Now the unit normal vector (eq. (28)) becomes

$$\hat{e}_n = -\sin\Gamma\,\hat{e}_x + \cos\Gamma\,(\cos\delta_\phi\,\hat{e}_r - \sin\delta_\phi\,\hat{e}_\phi) \tag{32}$$

As shown in fig. 4 the unit vector

$$\hat{e}_{NN} = \cos\delta_\phi\,\hat{e}_r - \sin\delta_\phi\,\hat{e}_\phi \tag{33}$$

is perpendicular to the curve of the body in a cross-sectional plane (but generally not normal to the body surface). Using eq. (33) in eq. (32), the unit

* For an axisymmetric body, $\frac{\partial f}{\partial \phi} \equiv 0$ and hence $\delta_\phi \equiv 0$.

normal vector can be written compactly as

$$\hat{e}_n = -\sin\Gamma\,\hat{e}_x + \cos\Gamma\,\hat{e}_{NN} \tag{34}$$

The unit vector tangent to the body curve in a cross-sectional plane (and also tangent to the body, see fig. 4) is

$$\hat{e}_T \equiv \hat{e}_x \times \hat{e}_{NN} = \cos\delta_\phi\,\hat{e}_\phi + \sin\delta_\phi\,\hat{e}_r \tag{35}$$

and the unit vector tangent to the body surface and normal to $\hat{e}_T$ is

$$\hat{e}_{11} \equiv \hat{e}_n \times \hat{e}_T = \cos\Gamma\,\hat{e}_x + \sin\Gamma\,\hat{e}_{NN} \tag{36}$$

Thus $\hat{e}_{11}$, $\hat{e}_n$, and $\hat{e}_T$ are a set of mutually perpendicular unit vectors with $\hat{e}_{11}$ and $\hat{e}_T$ tangent to the body surface.

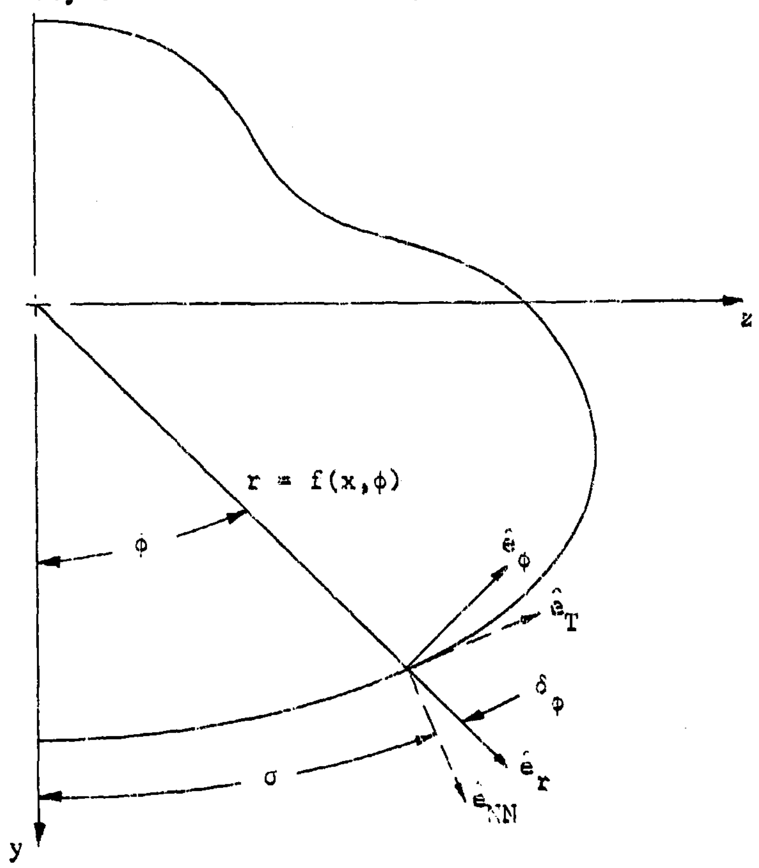

Figure 4. Rear view of body cross section

In order to determine the slope of an inviscid surface streamline, let $\hat{e}_s$ be a unit vector in the direction of the streamline with θ the angle between $\hat{e}_s$ and $\hat{e}_{11}$. Then

$$\hat{e}_s \equiv \cos\theta\,\hat{e}_{11} + \sin\theta\,\hat{e}_T \tag{37}$$

where $0 \leq \theta \leq \pi$ and it is easily verified that $\hat{e}_s \cdot \hat{e}_n = 0$. Define $\hat{e}_\beta$ as the unit vector tangent to the surface and normal to $\hat{e}_s$, i.e.

$$\hat{e}_\beta \equiv \hat{e}_s \times \hat{e}_n = -\sin\theta\,\hat{e}_{11} + \cos\theta\,\hat{e}_T \tag{38}$$

Here also $\hat{e}_s$, $\hat{e}_n$, and $\hat{e}_\beta$ are a set of mutually perpendicular unit vector with $\hat{e}_s$ and $\hat{e}_\beta$ tangent to the body surface. In terms of the unit vectors in cylindrical coordinates, eqs. (33), (35), and (36) may be used in eqs. (37) and (38) to write $\hat{e}_s$ and $\hat{e}_\beta$ as

$$\hat{e}_s = \cos\theta\cos\Gamma\,\hat{e}_x + (\sin\theta\sin\delta_\phi + \cos\theta\cos\delta_\phi\sin\Gamma)\hat{e}_r + (\sin\theta\cos\delta_\phi - \cos\theta\sin\delta_\phi\sin\Gamma)\hat{e}_\phi \tag{39}$$

and

$$\hat{e}_\beta = -\sin\theta\cos\Gamma\,\hat{e}_x + (\cos\theta\sin\delta_\phi - \sin\Gamma\sin\theta\cos\delta_\phi)\hat{e}_r + (\cos\theta\cos\delta_\phi + \sin\theta\sin\delta_\phi\sin\Gamma)\hat{e}_\phi \tag{40}$$

In order to trace out an inviscid surface streamline, it is first necessary to determine the angle θ along the streamline. This angle can be obtained from the inviscid momentum equations (Euler's equations) applied along the surface of the body.

Euler's equation may be written as

$$\frac{D\vec{V}}{Dt} = \frac{-\nabla p}{\rho}$$

where the operator $\frac{D}{Dt}$ is the time derivative along a streamline (for steady flows) and is related to the derivative D/DS as follows:

$$\frac{D}{Dt} = \frac{DS}{Dt}\frac{D}{DS} = V\frac{D}{DS}$$

where $\frac{D}{DS} = \frac{1}{h_s}\frac{\partial}{\partial\xi}$ is the derivative along a streamline and again $DS = dS = h_s\,d\xi$ is the differential of arc length along a streamline. With $\vec{V} = V\,\hat{e}_s$ the acceleration vector becomes

$$\frac{D\vec{V}}{Dt} = V\frac{D\vec{V}}{DS} = V\frac{DV}{DS}\,\hat{e}_s + V^2\frac{D\hat{e}_s}{DS} \tag{41}$$

The pressure gradient in streamline coordinates is

$$\nabla p = \frac{Dp}{DS}\,\hat{e}_s + \frac{1}{h}\frac{\partial p}{\partial \beta}\,\hat{e}_\beta + \frac{\partial p}{\partial n}\,\hat{e}_n \tag{42}$$

Thus Euler's equations become

$$V\frac{DV}{DS}\,\hat{e}_s + V^2\frac{D\hat{e}_s}{DS} = -\frac{1}{\rho}\left[\frac{Dp}{DS}\,\hat{e}_s + \frac{1}{h}\frac{\partial p}{\partial \beta}\,\hat{e}_\beta + \frac{\partial p}{\partial n}\,\hat{e}_n\right] \tag{43}$$

The scalar product of $\hat{e}_s$ with eq. (43) yields the familiar equation

$$V\frac{DV}{DS} = -\frac{1}{\rho}\frac{Dp}{DS} \tag{44}$$

where it is noted that

$$\frac{D\hat{e}_s}{DS}\cdot\hat{e}_s = 0$$

follows from $\hat{e}_s \cdot \hat{e}_s = 1$. Next, the scalar product of $\hat{e}_\beta$ with eq. (43) gives

$$V^2\frac{D\hat{e}_s}{DS}\cdot\hat{e}_\beta = -\frac{1}{\rho h}\frac{\partial p}{\partial \beta} \tag{45}$$

To evaluate the left side of this equation, the scalar product of $\hat{e}_\beta$ with the derivative of eq. (39) results in

$$d\hat{e}_s \cdot \hat{e}_\beta = d\theta + \sin\Gamma\, d\sigma \tag{46}$$

where

$$\sigma \equiv \phi - \delta_\phi \tag{47}$$

and the angle σ is shown on fig. 4.* Substitute eq. (46) into Eq. (45) to obtain

$$\frac{D\theta}{DS} + \sin\Gamma\,\frac{D\sigma}{DS} = -\frac{1}{\rho V^2}\frac{1}{h}\frac{\partial p}{\partial \beta} \tag{48}$$

This is the streamline equation in that it gives the angle θ along a streamline. However, before it can be applied, transformation operators are necessary to relate $\frac{D\sigma}{DS}$ and $\frac{1}{h}\frac{\partial p}{\partial \beta}$ to derivatives in cylindrical coordinates. These

---

* In obtaining eq. (46) from (39), note that $d\hat{e}_r = \hat{e}_\phi\, d\phi$ and $d\hat{e}_\phi = -\hat{e}_r\, d\phi$.

transformation operators are derived below.

Let $\vec{R}$ be the position vector of any point on the body surface relative to the origin of the cylindrical coordinate system ($x = 0$, $r = 0$). Since the body normal coordinate n is zero on the surface of the body where $r = f(x,\phi)$, the position vector can be written as $\vec{R} = \vec{R}(x,\phi)$ and thus

$$d\vec{R} = \frac{\partial \vec{R}}{\partial x} dx + \frac{\partial R}{\partial \phi} d\phi$$

$$= \hat{e}_x \, dx + \hat{e}_\phi \, f \, d\phi \qquad (49)$$

(see ref. 24). In terms of streamline coordinates on the body surface, the position vector can also be written as

$$\vec{R} = \vec{R}(\xi,\beta)$$

and thus

$$d\vec{R} = \frac{\partial \vec{R}}{\partial \xi} d\xi + \frac{\partial \vec{R}}{\partial \beta} d\beta$$

$$= \hat{e}_s \, h_s \, d\xi + \hat{e}_\beta \, h \, d\beta \qquad (50)$$

where

$$\frac{\partial \vec{R}}{\partial \xi} = \hat{e}_s \, h_s \qquad (51)$$

and

$$\frac{\partial \vec{R}}{\partial \beta} = \hat{e}_\beta \, h \qquad (52)$$

By equating the right side of eqs. (49) and (50), there results

$$\hat{e}_x \, dx + \hat{e}_\phi \, f \, d\phi = \hat{e}_s \, h_s \, d\xi + \hat{e}_\beta \, h \, d\beta \qquad (53)$$

The scalar product of this equation with $\hat{e}_x$ yields

$$dx = \hat{e}_s \cdot \hat{e}_x \, h_s \, d\xi + \hat{e}_\beta \cdot \hat{e}_x \, h \, d\beta$$

and since

$$dx = \frac{\partial x}{\partial \xi} d\xi + \frac{\partial x}{\partial \beta} d\beta$$

it follows that

$$\frac{\partial x}{\partial \xi} = \hat{e}_s \cdot \hat{e}_x \, h_s \qquad (54)$$

and

$$\frac{\partial x}{\partial \beta} = \hat{e}_\beta \cdot \hat{e}_x \, h \tag{55}$$

Similarly, the scalar product of $\hat{e}_\phi$ with eq. (53) provides

$$f d\phi = \hat{e}_s \cdot \hat{e}_\phi \, h_s \, d\xi + \hat{e}_\beta \cdot \hat{e}_\phi \, h \, d\beta$$

and therefore

$$f \frac{\partial \phi}{\partial \xi} = \hat{e}_s \cdot \hat{e}_\phi \, h_s \tag{56}$$

and

$$f \frac{\partial \phi}{\partial \beta} = \hat{e}_\phi \cdot \hat{e}_\beta \, h \tag{57}$$

Eqs. (54) to (57) may be used along with eqs. (39) and (40) to develop the transformation operators as

$$\begin{aligned}
\frac{1}{h}\frac{\partial}{\partial \beta} &= \frac{1}{h}\frac{\partial x}{\partial \beta}\frac{\partial}{\partial x} + \frac{1}{h}\frac{\partial \phi}{\partial \beta}\frac{\partial}{\partial \phi} \\
&= \hat{e}_x \cdot \hat{e}_\beta \frac{\partial}{\partial x} + \frac{\hat{e}_\phi \cdot \hat{e}_\beta}{f}\frac{\partial}{\partial \phi} \\
&= -\sin\theta \cos\Gamma \frac{\partial}{\partial x} + \frac{(\cos\theta \cos\delta_\phi + \sin\theta \sin\delta_\phi \sin\Gamma)}{f}\frac{\partial}{\partial \phi}
\end{aligned} \tag{58}$$

and

$$\begin{aligned}
\frac{D}{DS} &= \frac{1}{h_s}\frac{\partial}{\partial \xi} = \frac{1}{h_s}\frac{\partial x}{\partial \xi}\frac{\partial}{\partial x} + \frac{1}{h_s}\frac{\partial \phi}{\partial \xi}\frac{\partial}{\partial \phi} \\
&= \hat{e}_x \cdot \hat{e}_s \frac{\partial}{\partial x} + \frac{\hat{e}_\phi \cdot \hat{e}_s}{f}\frac{\partial}{\partial \phi} \\
&= \cos\theta \cos\Gamma \frac{\partial}{\partial x} + \frac{(\sin\theta \cos\delta_\phi - \cos\theta \sin\delta_\phi \sin\Gamma)}{f}\frac{\partial}{\partial \phi}
\end{aligned} \tag{59}$$

In the equations above it is implied that all derivatives are evaluated on the body where $r = f(x,\phi)$ and $n = 0$; thus

$$\frac{\partial}{\partial x} = \left(\frac{\partial}{\partial x}\right)_{\phi,n} \qquad \text{and} \qquad \frac{\partial}{\partial \phi} = \left(\frac{\partial}{\partial \phi}\right)_{x,n}$$

The transformation operators given by eqs. (58) and (59) can now be used to write the streamline equation (eq. (48)) in its final form as

$$\frac{D\theta}{DS} = -\left(\frac{p_s}{\rho_s V_\infty^2}\right)\left(\frac{\rho_s}{\rho}\frac{V_\infty^2}{V^2}\right)\left[-\sin\theta\cos\Gamma\frac{\partial}{\partial x}\left(\frac{p}{p_s}\right) + \frac{(\cos\theta\cos\delta_\phi + \sin\theta\sin\delta_\phi\sin\Gamma)}{f}\frac{\partial}{\partial\phi}\left(\frac{p}{p_s}\right)\right]$$
$$- \sin\Gamma\left[\cos\theta\cos\Gamma\frac{\partial\sigma}{\partial x} + \frac{(\sin\theta\cos\delta_\phi - \cos\theta\sin\delta_\phi\sin\Gamma)}{f}\frac{\partial\sigma}{\partial\phi}\right] \tag{60}$$

For a given surface pressure distribution, whether experimental or theoretical, this equation can be integrated numerically to determine θ along a streamline emanating from the stagnation point. However, eq. (60) is indeterminate at the stagnation point, and this topic is covered below under the sub-heading Stagnation Region Streamlines. The density ρ and speed V may be obtained from the pressure and entropy by use of isentropic relations for a perfect gas or equilibrium air. The geometric location of each integration step along the streamline is calculated by numerically integrating eqs. (54) and (56), which by the use of eq. (39) become

$$\frac{Dx}{DS} = \cos\theta\cos\Gamma \tag{61}$$

and

$$\frac{D\phi}{DS} = \frac{\sin\theta\cos\delta_\phi - \cos\theta\sin\delta_\phi\sin\Gamma}{f} \tag{62}$$

Since the surface streamlines and their corresponding orthogonal lines are curvilinear, the scale factors (metric coefficients) h_s and h play an important role because in the relation $dS = h_s\, d\xi$ the quantity $d\xi$ is an exact differential whereas dS in general is not. Likewise $d\beta$ is an exact differential whereas the quantity $dq = h\, d\beta$ is not. The importance of this statement lies in the fact that since $d\xi$ and $d\beta$ are exact differentials, mixed partial derivatives are interchangeable, i.e.

$$\frac{\partial^2 \vec{R}}{\partial\xi\partial\beta} = \frac{\partial^2 \vec{R}}{\partial\beta\partial\xi}$$

whereas it is noted that

$$\frac{\partial^2 \vec{R}}{\partial S \partial q} \neq \frac{\partial^2 \vec{R}}{\partial q \partial S}$$

From eqs. (51) and (52) there results

$$\frac{\partial^2 \vec{R}}{\partial \xi \partial \beta} = \frac{\partial}{\partial \xi} \frac{\partial \vec{R}}{\partial \beta} = \frac{\partial}{\partial \xi} (h\ \hat{e}_\beta)$$

and

$$\frac{\partial^2 \vec{R}}{\partial \beta \partial \xi} = \frac{\partial}{\partial \beta} \frac{\partial \vec{R}}{\partial \xi} = \frac{\partial}{\partial \beta} (h_s\ \hat{e}_s)$$

By equating the right side of the two equations above, it follows that

$$\frac{\partial}{\partial \xi} (h\ \hat{e}_\beta) = \frac{\partial}{\partial \beta} (h_s\ \hat{e}_s)$$

which upon expanding becomes

$$\frac{\partial h}{\partial \xi} \hat{e}_\beta + h \frac{\partial \hat{e}_\beta}{\partial \xi} = \frac{\partial h_s}{\partial \beta} \hat{e}_s + h_s \frac{\partial \hat{e}_s}{\partial \beta} \tag{63}$$

The scalar product of $\hat{e}_\beta$ with the equation above yields*

$$\frac{\partial h}{\partial \xi} = h_s \frac{\partial \hat{e}_s}{\partial \beta} \cdot \hat{e}_\beta$$

The equation above may be combined with eq. (46) and the relation $dS = h_s\ d\xi$ to give

$$\frac{Dh}{DS} = \frac{\partial \theta}{\partial \beta} + \sin \Gamma \frac{\partial \sigma}{\partial \beta} \tag{64}$$

This equation cannot be used to calculate the scale factor h along a streamline because $\frac{\partial \theta}{\partial \beta}$ is unknown when only surface pressures are given.

In order to obtain an equation for the scale factor h, rewrite eq. (48) as

$$-\frac{h_s}{\rho V^2 h} \frac{\partial p}{\partial \beta} = \frac{\partial \theta}{\partial \xi} + \sin \Gamma \frac{\partial \sigma}{\partial \xi} \tag{48}$$

*As before, $\frac{\partial \hat{e}_\beta}{\partial \xi} \cdot \hat{e}_\beta = 0$ follows from $\hat{e}_\beta \cdot \hat{e}_\beta = 1$

Differentiate this equation with respect to β and substract the result from the derivative of eq. (64) with respect to ξ to get

$$\frac{1}{h}\frac{D^2h}{DS^2} = -\frac{1}{h_s h}\frac{\partial}{\partial\beta}\left[\frac{h_s}{\rho V^2 h}\frac{\partial p}{\partial\beta}\right] + \frac{D(\sin\Gamma)}{DS}\frac{\partial\sigma}{h\partial\beta}$$

$$-\frac{D\sigma}{DS}\frac{\partial(\sin\Gamma)}{h\partial\beta} \qquad (65)$$

where the equalities

$$\frac{\partial^2\theta}{\partial\xi\partial\beta} = \frac{\partial^2\theta}{\partial\beta\partial\xi} \qquad \text{and} \qquad \frac{\partial^2\sigma}{\partial\xi\partial\beta} = \frac{\partial^2\sigma}{\partial\beta\partial\xi}$$

were used to obtain eq. (65). This is the differential equation to be integrated along a streamline to determine the scale factor h; however the terms on the right side of eq. (65) must first be cast into a usable form.

By use of the transformation operators from eqs. (58) and (59), it is found that the last two terms in eq. (65) may be expressed as

$$\frac{D(\sin\Gamma)}{DS}\frac{\partial\sigma}{h\partial\beta} - \frac{D\sigma}{DS}\frac{\partial(\sin\Gamma)}{h\partial\beta} = \frac{\cos^2\Gamma\cos\delta_\phi}{f}\left[\frac{\partial\Gamma}{\partial x}\frac{\partial\sigma}{\partial\phi} - \frac{\partial\sigma}{\partial x}\frac{\partial\Gamma}{\partial\phi}\right] \qquad (66)$$

and the first term on the right side of eq. (65) may be expanded to give

$$\frac{1}{h_s h}\frac{\partial}{\partial\beta}\left(\frac{h_s}{\rho V^2 h}\frac{\partial p}{\partial\beta}\right) = \left(\frac{1}{h_s h}\frac{\partial h_s}{\partial\beta}\right)\left(\frac{1}{\rho V^2 h}\frac{\partial p}{\partial\beta}\right)$$

$$-\frac{1}{h}\frac{\partial p}{\partial\beta}\frac{1}{\rho^2 V^2 h}\frac{\partial\rho}{\partial\beta} - \frac{1}{h}\frac{\partial p}{\partial\beta}\frac{1}{\rho V^4}\frac{1}{h}\frac{\partial V^2}{\partial\beta}$$

$$+\frac{1}{\rho V^2}\frac{1}{h}\frac{\partial}{\partial\beta}\left(\frac{1}{h}\frac{\partial p}{\partial\beta}\right) \qquad (67)$$

The four terms on the right side of eq. (67) are evaluated below.

Take the scalar product of $\hat{e}_s$ with eq. (63) to get

$$h\frac{\partial\hat{e}_\beta}{\partial\xi}\cdot\hat{e}_s = \frac{\partial h_s}{\partial\beta} \qquad (68)$$

Since $\hat{e}_\beta \cdot \hat{e}_s = 0$, then

$$\frac{\partial \hat{e}_\beta}{\partial \xi} \cdot \hat{e}_s = - \frac{\partial \hat{e}_s}{\partial \xi} \cdot \hat{e}_\beta \tag{69}$$

and eqs. (46) and (69) may be combined with eq. (68) to yield

$$- h \left[\frac{\partial \theta}{\partial \xi} + \sin \Gamma \frac{\partial \sigma}{\partial \xi} \right] = \frac{\partial h_s}{\partial \beta} \tag{70}$$

Comparing this equation with eq. (48), it is seen that the term $\frac{1}{h_s h} \frac{\partial h_s}{\partial \beta}$ in eq. (67) becomes

$$\frac{1}{h_s h} \frac{\partial h_s}{\partial \beta} = \frac{1}{\rho V^2 h} \frac{\partial p}{\partial \beta} \tag{71}$$

Since the inviscid flow along the surface is isentropic, $p = p(\rho, \bar{S})$ and the term $\frac{V^2}{h} \frac{\partial \rho}{\partial \beta}$ in eq. (67) can be expressed as

$$\frac{V^2}{h} \frac{\partial \rho}{\partial \beta} = \frac{V^2}{\left(\frac{\partial p}{\partial \rho}\right)_{\bar{s}}} \frac{1}{h} \frac{\partial p}{\partial \beta} = M^2 \frac{1}{h} \frac{\partial p}{\partial \beta} \tag{72}$$

The Bernoulli equation $\rho V \, dV = - dp$ along the surface allows the term $\frac{1}{h} \frac{\partial V^2}{\partial \beta}$ in eq. (67) to be written as

$$\frac{1}{h} \frac{\partial V^2}{\partial \beta} = 2 \frac{V}{h} \frac{\partial V}{\partial \beta} = - \frac{2}{\rho h} \frac{\partial p}{\partial \beta} \tag{73}$$

The fourth and last term to be evaluated for eq. (67) is $\frac{1}{h} \frac{\partial}{\partial \beta} \left[\frac{1}{h} \frac{\partial p}{\partial \beta} \right]$. By repeated application of the transformation operator of eq. (58) the following relation is obtained:

$$\begin{aligned} \frac{1}{h} \frac{\partial}{\partial \beta} \left[\frac{1}{h} \frac{\partial p}{\partial \beta} \right] = & \left[\frac{1}{h} \frac{Dh}{DS} - \frac{\sin \Gamma}{h} \frac{\partial \sigma}{\partial \beta} \right] \left[- \frac{Dp}{DS} \right] + \sin \theta \sin \Gamma \frac{\partial p}{\partial x} \frac{1}{h} \frac{\partial \Gamma}{\partial \beta} \\ & + \frac{1}{f} \frac{\partial p}{\partial \phi} \Big[\sin \theta \sin \delta_\phi \cos \Gamma \frac{1}{h} \frac{\partial \Gamma}{\partial \beta} + (-\cos \theta \sin \delta_\phi \\ & + \sin \theta \cos \delta_\phi \cos \Gamma) \left(\frac{1}{h} \frac{\partial \delta_\phi}{\partial \beta} + \frac{\hat{e}_\beta \cdot \hat{e}_\phi}{f} \right) \Big] + \sin^2 \theta \cos^2 \Gamma \frac{\partial^2 p}{\partial x^2} \\ & - 2 \sin \theta \cos \Gamma (\hat{e}_\beta \cdot \hat{e}_\phi) \frac{1}{f} \frac{\partial^2 p}{\partial x \partial \phi} + (\hat{e}_\beta \cdot \hat{e}_\phi)^2 \frac{1}{f^2} \frac{\partial^2 p}{\partial \phi^2} \end{aligned} \tag{74}$$

In order to obtain eq. (74), eq. (64) was used to substitute for $\frac{1}{h}\frac{\partial\theta}{\partial\beta}$, the term $\hat{e}_\beta \cdot \hat{e}_\phi$ follows from eq. (40) as

$$\hat{e}_\beta \cdot \hat{e}_\phi = \cos\theta \cos\delta_\phi + \sin\theta \sin\delta_\phi \sin\Gamma \tag{75}$$

and eq. (58) was used to write

$$\frac{1}{h}\frac{\partial f}{\partial\beta} = \cos\theta \sin\delta_\phi - \sin\theta \sin\Gamma \cos\delta_\phi \tag{76}$$

Using the results from eqs. (66) through (73), the equation for the scale factor h (eq. (65)) becomes

$$\frac{1}{h}\frac{D^2h}{DS^2} = -\left[\frac{p_s}{\rho_s V_\infty^2}\frac{\rho_s}{\rho}\frac{V_\infty^2}{V^2}\frac{1}{h}\frac{\partial}{\partial\beta}(p/p_s)\right]^2(3 - M^2)$$
$$+ \frac{p_s}{\rho_s V_\infty^2}\frac{\rho_s}{\rho}\frac{V_\infty^2}{V^2}\frac{1}{h}\frac{\partial}{\partial\beta}\left[\frac{1}{h}\frac{\partial}{\partial\beta}(p/p_s)\right]$$
$$+ \frac{\cos^2\Gamma \cos\delta_\phi}{f}\left[\frac{\partial\Gamma}{\partial x}\frac{\partial\sigma}{\partial\phi} - \frac{\partial\sigma}{\partial x}\frac{\partial\Gamma}{\partial\phi}\right] \tag{75}$$

Eq. (74) is used in the center term on the right side of eq. (75), and the transformation operators of eqs. (58) and (59) are used to transform partial derivatives from streamline coordinates to cylindrical coordinates.

The geodesic curvature of a curve ξ = constant on the body surface is

$$\frac{1}{h}\frac{Dh}{DS}$$

and it is a measure of the amount that the streamlines converge or diverge. If $\frac{Dh}{DS}$ is positive h increases along the streamline, and two neighboring streamlines move further apart, i.e. the streamlines diverge. Conversely, if the streamlines converge $\frac{Dh}{DS}$ is negative. As indicated in ref. 6, the form of eq. (75) shows that h is not completely determinate. It may be multiplied by a constant or any function of β. However, changes in h will also result in changes in β. For the analysis here it is convenient to choose h and β in such a way that they reduce to the radius r and the circumferential angle ϕ, respectively, for the special case of an axisymmetric body at zero angle-of-attack. Thus β will be dimensionless, and h will have the dimensions of a length.

In summary, the inviscid surface streamlines and their corresponding scale factor h are calculated by numerically integrating eqs. (60), (61), (62), and (75) for θ, x, ϕ, and h, respectively, along each streamline. The numerical integration scheme used here is the 4th order variable step-size Runge-Kutta method. Initial conditions required to start the integration of each streamline are developed below in the section on Stagnation Region Streamlines. See the Appendix for additional information on h.

It can be shown that eqs. (64) and (70) are the same as the Mainardi-Codazzi relations in ref. 24, and eq. (65) is equivalent to the Gauss characteristic equation in ref. 24.

Simplified Streamlines

A simplified method of approximating the streamline direction on the body surface was used with good success by DeJarnette and Davis (ref. 14) in calculating laminar heating rates over blunt-nosed cones at an angle of attack. In this method it is assumed that the direction of an inviscid surface streamline is given by the resultant of the free-stream velocity vector minus its component normal to the surface*. This assumption was motivated by the fact that in the Newton-Busemann theory the initial direction of a particle entering the shock layer is in the direction of these simplified streamlines. However, the Newton-Busemann theory has the particles following surface geodesics after entering the shock layer, which differ from the simplified streamlines (see ref. 7). The simplified streamlines described here are called the method of steepest descent in ref. 7 and Newtonian streamlines in ref. 9. DeJarnette and Tai (ref. 15) found that the simplified streamlines could be used to calculate reasonably accurate laminar heating rates for some cases even when the streamlines themselves were inaccurate. Simplified streamlines are developed here as an alternate method for calculating the inviscid surface streamlines and corresponding scale factor.

---

* The magnitude of the velocity, however, is calculated from the surface pressure and entropy.

Define $\hat{V}_\infty$ as a unit vector in the direction of the free-stream velocity vector, then the simplified method gives the direction of a streamline by the equation

$$\hat{e}_s \equiv \frac{\hat{V}_\infty - (\hat{V}_\infty \cdot \hat{e}_n)\hat{e}_n}{|\hat{V}_\infty - (\hat{V}_\infty \cdot \hat{e}_n)\hat{e}_n|} = \frac{\hat{e}_n \times (\hat{V}_\infty \times \hat{e}_n)}{|\hat{e}_n \times (\hat{V}_\infty \times \hat{e}_n)|} \tag{76}$$

With $\hat{V}_\infty$ in the body plane of symmetry (x - y plane), it can be expressed as (see fig. 3)

$$\hat{V}_\infty = \cos\alpha\, \hat{e}_x - \sin\alpha\, (\hat{e}_r \cos\phi - \hat{e}_\phi \sin\phi) \tag{77}$$

where the term in parentheses is the unit vector in the y-direction. Using eqs. (32) and (77), the angle ψ is given by

$$\cos\psi \equiv -\hat{V}_\infty \cdot \hat{e}_n = \cos\alpha \sin\Gamma + \sin\alpha \cos\Gamma \cos\sigma \tag{78}$$

where $0 \leq \psi \leq \pi$. It then follows that

$$|\hat{e}_n \times (\hat{V}_\infty \times \hat{e}_n)| = |\hat{V}_\infty \times \hat{e}_n| = \sin\psi \tag{79}$$

and eq. (76) becomes

$$\hat{e}_s = \frac{\hat{V}_\infty + \cos\psi\, \hat{e}_n}{\sin\psi} \tag{80}$$

To determine the streamline direction in terms of θ, equate the expressions for $\hat{e}_s$ given by eqs. (39) and (80) to get

$$\sin\theta = \frac{\sin\alpha \sin\sigma}{\sin\psi} \tag{81}$$

and also

$$\cos\theta = \frac{\cos\alpha - \cos\psi \sin\Gamma}{\cos\Gamma \sin\psi} = \frac{\cos\alpha \cos\Gamma - \sin\alpha \sin\Gamma \cos\sigma}{\sin\psi} \tag{82}$$

$(0 \leq \theta \leq \pi)$

These equations along with eqs. (61) and (62) are used to compute the streamline geometry by the simplified method. In contrast to the previous section, which calculated θ from a differential equation involving the surface pressure distribution, eq. (82) allows θ to be determined at any position on the body without integrating a differential equation from the stagnation point to the point in question.

It remains to develop an equation for the scale factor h corresponding to the simplified streamlines. Recall that eq. (64) was

$$\frac{Dh}{DS} = \frac{\partial \theta}{\partial \beta} + \sin \Gamma \frac{\partial \sigma}{\partial \beta} \tag{64}$$

This equation can be used here to calculate h because the term $\frac{\partial \theta}{\partial \beta}$ can be determined as follows. Differentiate eq. (78) to obtain

$$- \sin \psi \frac{\partial \psi}{\partial \beta} = (\cos \alpha \cos \Gamma - \sin \alpha \sin \Gamma \cos \sigma) \frac{\partial \Gamma}{\partial \beta}$$

$$- \sin \alpha \cos \Gamma \sin \sigma \frac{\partial \sigma}{\partial \beta} \tag{83}$$

and by using eqs. (81) and (82) this equation becomes

$$\frac{\partial \psi}{\partial \beta} = - \cos \theta \frac{\partial \Gamma}{\partial \beta} + \cos \Gamma \sin \theta \frac{\partial \sigma}{\partial \beta} \tag{84}$$

Next, differentiate eq. (82) with respect to β and substitute eq. (84) for $\frac{\partial \psi}{\partial \beta}$ to get

$$\frac{\partial \theta}{\partial \beta} = \frac{\cos \psi}{\sin \psi} (\sin \theta \frac{\partial \Gamma}{\partial \beta} + \cos \theta \cos \Gamma \frac{\partial \sigma}{\partial \beta}) - \sin \Gamma \frac{\partial \sigma}{\partial \beta} \tag{85}$$

Substitute eq. (85) into (64) to obtain

$$\frac{1}{h} \frac{Dh}{DS} = \frac{\cos \psi}{\sin \psi} \left[\sin \theta \frac{1}{h} \frac{\partial \Gamma}{\partial \beta} + \cos \theta \cos \Gamma \frac{1}{h} \frac{\partial \sigma}{\partial \beta} \right]. \tag{86}$$

Then using the transformation operator of eq. (58) for $\frac{1}{h} \frac{\partial}{\partial \beta}$ on the right side, this first-order differential equation can be integrated along a simplified streamline to determine the corresponding scale factor. Note, however, that both eqs. (81) and (86) are indeterminate at the stagnation point, and the analysis in the section below must be used to supply the initial conditions for each streamline. Although this method of computing simplified streamlines should only be used on the windward side of the body, it was also used on the leeward side in reference 14 with reasonably good results for the corresponding heating rates.

Stagnation Region Streamlines

The equations developed previously for the inviscid surface streamlines and scale factor h are singular at the stagnation point. In fact it will be shown below that this is a nodal point. Therefore, an analytic solution will be developed for a small region surrounding the stagnation point. This solution will then provide initial conditions to start the numerical integration of the differential equations for the streamline geometry and corresponding scale factor h given in the previous two sections.

The actual location of the true stagnation point would require a numerical solution of the inviscid flow field over these three-dimensional bodies at an angle of attack. However, the true stagnation point is generally close to the Newtonian stagnation point for blunt-nosed bodies. Therefore, to be consistent with both the modified Newtonian pressure distribution and the simplified streamlines, the Newtonian stagnation point will be used in the analysis here. This point is determined by the position on the windward side of the body where

$$\hat{V}_\infty \cdot \hat{e}_n = -1$$

This condition requires that $\Gamma = \frac{\pi}{2} - \alpha$, and when $\alpha > 0$ symmetry dictates that $\phi = 0$ and $\delta_\phi = 0$ at the stagnation point.

For the region surrounding the stagnation point, it is advantageous to use coordinates S_{11} and S_T which are along the body surface and in the directions of $\hat{e}_{11}$ and $\hat{e}_T$, respectively. These unit vectors were defined by eqs. (35) and (36), and figure 5 illustrates these quantities.

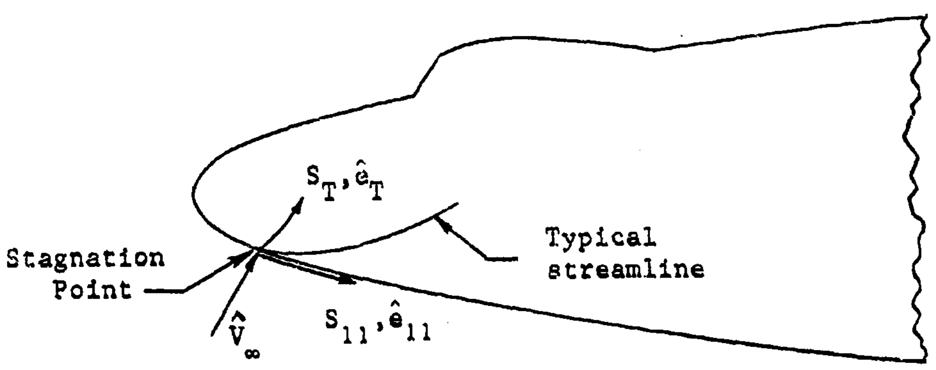

Figure 5.- Stagnation region coordinates

The coordinate S_{11} is along the windward streamline (in the plane of symmetry), whereas S_T is normal to S_{11} but on the body surface.

Consider again the position vector, $\vec{R}$, relative to the nose of the body ($x = 0$, $r = 0$) as used previously. Then $\vec{R}$ can be considered a function of the streamline coordinates (ξ,β) or the surface coordinates (S_{11},S_T). It follows that

$$d\vec{R} = \frac{\partial \vec{R}}{\partial \xi} d\xi + \frac{\partial \vec{R}}{\partial \beta} d\beta = \frac{\partial \vec{R}}{\partial S_{11}} dS_{11} + \frac{\partial \vec{R}}{\partial S_T} dS_T$$

$$= h_s d\xi\, \hat{e}_s + h d\beta\, \hat{e}_\beta = dS_{11}\, \hat{e}_{11} + dS_T\, \hat{e}_T \tag{87}$$

where it should be noted that dS_{11} and dS_T are not exact differentials.

Take the scalar product of $\hat{e}_{11}$ with the equation above to get (using $dS = h_s d\xi$)

$$dS_{11} = dS\, \hat{e}_s \cdot \hat{e}_{11} + h\, d\beta\, \hat{e}_\beta \cdot \hat{e}_{11} \tag{88}$$

Recall that $\frac{D}{DS} = \left[\frac{\partial}{\partial S}\right]_\beta$; hence by using eq. (37) it follows from eq. (88) that

$$\frac{DS_{11}}{DS} = \hat{e}_s \cdot \hat{e}_{11} = \cos\theta \tag{89}$$

In a similar manner it is found that

$$\frac{DS_T}{DS} = \hat{e}_s \cdot \hat{e}_T = \sin\theta \tag{90}$$

which when combined with the previous equation yields

$$\frac{DS_T}{DS_{11}} = \tan\theta \tag{91}$$

The inviscid surface velocity vector can be written as

$$\vec{V} = V\, \hat{e}_s = V_{11}\, \hat{e}_{11} + V_T\, \hat{e}_T \tag{92}$$

Considering $V_{11} = V_{11}(S_{11}, S_T)$ and $V_T = V_T(S_{11}, S_T)$, the stagnation point ($S_{11} = 0$ and $S_T = 0$) requires that $V_{11}(0, 0) = V_T(0, 0) = 0$, and due to symmetry,

$$\frac{\partial V_{11}(S_{11}, 0)}{\partial S_T} = 0 \qquad \text{and} \qquad V_T(S_{11}, 0) = 0$$

Therefore, for the region near the stagnation point,

$$V_{11} \approx \left[\frac{\partial V_{11}}{\partial S_{11}}\right]_s S_{11} \quad \text{and} \quad V_T \approx \left[\frac{\partial V_T}{\partial S_T}\right]_s S_T$$

and the equation of a streamline in this region can be written as

$$\frac{DS_T}{DS_{11}} = \frac{\left[\frac{DS_T}{Dt}\right]}{\left[\frac{DS_{11}}{Dt}\right]} = \frac{V_T}{V_{11}} \approx \frac{\left[\frac{\partial V_T}{\partial S_T}\right]_s}{\left[\frac{\partial V_{11}}{\partial S_{11}}\right]_s} \frac{S_T}{S_{11}} \tag{93}$$

Define $B \equiv \frac{\left[\frac{\partial V_{11}}{\partial S_{11}}\right]_s}{\left[\frac{\partial V_T}{\partial S_T}\right]_s}$ as the ratio of the principal velocity gradients at the stagnation point. Then eq. (93) becomes

$$\frac{DS_T}{DS_{11}} = \frac{1}{B} \frac{S_T}{S_{11}} \tag{94}$$

which may be integrated to yield

$$S_{11} = C(\beta)\, S_T^B \tag{95}$$

where the "constant" of integration $C(\beta)$ is really a function of β since the derivative $\frac{DS_T}{DS_{11}}$ implies β is held constant. The parameter $C(\beta)$ distinguishes one streamline from another because β is constant along a streamline. For convex bodies $B > 0$, and eq. (95) indicates that the stagnation point is a nodal point. When the stagnation region is spherical, $B = 1$ and the streamlines emanate radially from the stagnation point. For $B \neq 1$, the streamlines do not emanate radially from the stagnation point, and the slope of the streamlines at the stagnation point is obtained from eqs. (91) and (95) as

$$\tan\theta_s = \left[\frac{DS_T}{DS_{11}}\right]_s = \lim_{S_T \to 0} \left[\frac{S_T^{\,1-B}}{B\, C(\beta)}\right] \tag{96}$$

Hence, for $C(\beta)$ finite and non-zero, the slope of a streamline at the stagnation point is $\tan\theta_s = 0$ for $B < 1$ or $\tan\theta_s \to \infty$ for $B > 1$; whereas for $B = 1$ (sphere) $\tan\theta_s \to \frac{1}{C(\beta)}$ which gives an infinite number of values as β changes from one streamline to another. It will be shown later that by the use of modified Newtonian pressures B becomes the ratio of the two principal radii of curvature at the stagnation point.

In order to evaluate $C(\beta)$, consider the developed region around the stagnation point, as shown in figure 6.

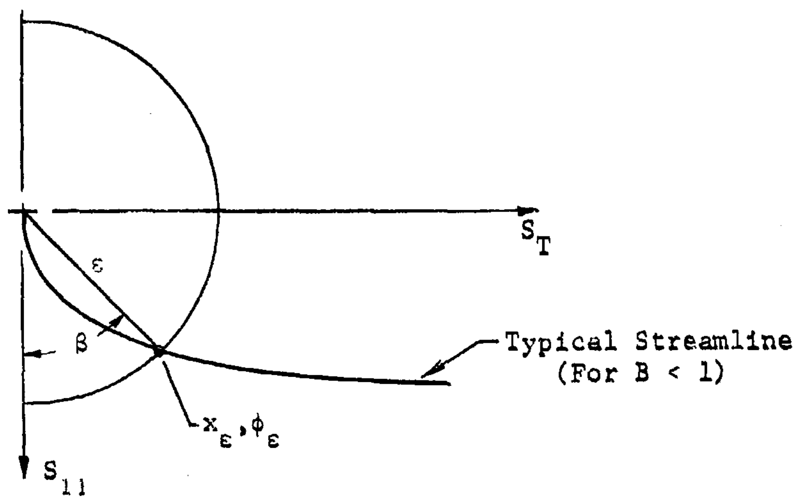

Figure 6. Stagnation region

On the circle of radius ε, corresponding to the point where a streamline crosses this circle, the angle β is assigned as shown in figure 6. Also, on this circle the coordinates of the streamline are $S_{11} = \varepsilon \cos\beta$ and $S_T = \varepsilon \sin\beta$. Now the streamline equation $S_{11} = C(\beta)\, S_T^B$ is assumed to hold throughout this circular region. Applying this equation at the point where the streamline crosses the circle yields

$$\varepsilon \cos\beta = C(\beta)(\varepsilon \sin\beta)^B$$

which gives

$$C(\beta) = \frac{\varepsilon \cos\beta}{(\varepsilon \sin\beta)^B} \tag{97}$$

Thus the parameter $C(\beta)$ also depends on the value of ε chosen.

The equation for the streamlines is now

$$\frac{S_{11}}{\varepsilon} = \frac{\cos\beta}{\sin^B\beta}\left[\frac{S_T}{\varepsilon}\right]^B \tag{98}$$

Different values of $0 \le \beta \le \pi$ yield different streamlines. The slope of a streamline follows from eqs. (91) and (98) as

$$\tan\theta = \frac{DS_T}{DS_{11}} = \frac{\sin^B\beta}{B\cos\beta}(S_T/\varepsilon)^{1-B} \tag{99}$$

and for θ_ε the value of θ on the ε circle, where $S_T = \varepsilon\sin\beta$, the equation above gives

$$\tan\theta_\varepsilon = \frac{\tan\beta}{B} \tag{100}$$

Hence for $B \neq 1$, $\theta_\varepsilon \neq \beta$; whereas for the sphere ($B = 1$) $\theta_\varepsilon = \beta$ (radial streamlines). The windward streamline is $\beta = 0$ and the leeward is $\beta = 180°$.

Next, consider the evaluation of the scale factor, h, in this region surrounding the stagnation point. Take the scalar product of $\hat{e}_\beta$ with equation (87) to get

$$h d\beta = dS_{11}\,\hat{e}_{11}\cdot\hat{e}_\beta + dS_T\,\hat{e}_T\cdot\hat{e}_\beta$$

Considering $\beta = \beta(S_{11}, S_T)$, the previous equation gives

$$h\frac{\partial\beta}{\partial S_T} = \hat{e}_T\cdot\hat{e}_\beta = \cos\theta$$

Hence $$h = \frac{\cos\theta}{\frac{\partial\beta}{\partial S_T}} \tag{101}$$

The derivative $\frac{\partial\beta}{\partial S_T}$ is obtained by differentiating eq. (98), and the result is

$$\frac{\partial\beta}{\partial S_T} = \frac{B\cos\beta\sin\beta}{S_T(\sin^2\beta + B\cos^2\beta)} \tag{102}$$

The term $\cos\theta$ may be obtained from equation (99) as

$$\cos\theta = \frac{B\cos\beta}{\left[B^2\cos^2\beta + \sin^{2B}\beta\left(\frac{S_T}{\varepsilon}\right)^{2B-2}\right]^{1/2}} \tag{103}$$

Substituting eqs. (102) and (103) into eq. (101) yields the following equation for the scale factor

$$h = \frac{(\sin^2\beta + B\cos^2\beta)S_T}{\left[B^2\cos^2\beta + \sin^{2B}\beta\left(\frac{S_T}{\varepsilon}\right)^{2-2B}\right]^{1/2}\sin\beta} \tag{104}$$

On the circle of radius ε, where $S_T = \varepsilon\sin\beta$, the scale factor becomes

$$h_\varepsilon = \frac{(\sin^2\beta + B\cos^2\beta)\varepsilon}{(\sin^2\beta + B^2\cos^2\beta)^{1/2}} \tag{105}$$

For later use, $\left[\frac{Dh}{DS}\right]_\varepsilon$ is needed, and this quantity can be determined from the derivative of eq. (104). The result is

$$\left[\frac{Dh}{DS}\right]_\varepsilon = B\left[\frac{\sin^2\beta + B\cos^2\beta}{\sin^2\beta + B^2\cos^2\beta}\right]^2 \tag{106}$$

Again, it is worth noting that for a spherical region $B = 1$ and eqs. (105) and (106) give

$$h_\varepsilon = \varepsilon \quad \text{and} \quad \left[\frac{Dh}{DS}\right]_\varepsilon = 1$$

which to first order are correct.

As shown by Reshotko, ref. 25, the ratio of velocity gradients, B, may be evaluated from modified Newtonian theory as

$$B = \frac{R_T}{R_{11}} \tag{107}$$

where

$$R_T = \left[\frac{f}{\cos\Gamma\,\frac{\partial\sigma}{\partial\phi}}\right]_s \tag{108}$$

is the surface radius of curvature in the S_T direction, and

$$R_{11} = -\left[\frac{1}{\cos\Gamma\,\frac{\partial\Gamma}{\partial x}}\right]_s \tag{109}$$

is the surface radius of curvature in the S_{11} direction, both at the stagnation point.

The location of each streamline on the ε circle is determined by purely geometrical considerations. Suppose the stagnation region inside the ε circle is represented by part of an ellipsoid with principal radii of curvature given by R_T and R_{11}. Then for $\varepsilon/R_T << 1$ the coordinates of a streamline on the ε circle are:

$$x_\varepsilon = x_s + \varepsilon[\cos\beta \sin\alpha + \frac{\varepsilon}{R_T} \frac{\cos\alpha}{2} (\sin^2\beta + B\cos^2\beta)] \tag{110}$$

$$y_\varepsilon = f_s + \varepsilon[\cos\beta \cos\alpha - \frac{\varepsilon}{R_T} \frac{\sin\alpha}{2} (\sin^2\beta + B\cos^2\beta)] \tag{111}$$

$$z_\varepsilon = \varepsilon \sin\beta \tag{112}$$

$$\phi_\varepsilon = \tan^{-1} (z_\varepsilon/y_\varepsilon) \tag{113}$$

Note that the form of the above equations causes no difficulty at $\alpha = 0$.

In choosing a value for ε, a compromise between accuracy and computational time must be made. The smaller the value of ε the more accurate eqs. (110) through (113) become. On the other hand, it was found that the step size used to start the numerical integration of the streamline equations outside the ε circle must be less than about $\varepsilon/10$. After testing several values of ε, a value in the range $0.01 < \varepsilon/R_T < 0.1$ was found to be sufficiently small to make eqs. (110) through (113) reasonably accurate, yet large enough to keep the integration step size for the streamline equations from becoming prohibitively small.

Surface Pressure Distribution

As mentioned previously, the calculation of the inviscid surface streamlines and heating rates are dependent on the surface pressure distribution. Two options are considered here for the pressure distribution, depending on whether pressure data from another source is available or not. First, if experimental or theoretical pressures (ratioed to stagnation pressure) are known, tabulated values around the circumference at several axial stations are used to generate a two-dimensional spline function for the pressure ratios and derivatives at any position on the body. This two-dimensional spline function is similar to that used to describe the body geometry except for the axial variation. For blunt-nosed bodies, $\frac{\partial p}{\partial x} \to \infty$ at $x = 0$ but $\frac{\partial p}{\partial \sqrt{x}}$ is finite there. Therefore, the pressure spline function is developed to vary with $\sqrt{x}$ in the axial direction. For a given circumferential angle ϕ the derivative $\frac{\partial p}{\partial \sqrt{x}}$ for both $x = 0$ and the end of the body is determined by the derivative from Lagrangian interpolation.

When surface pressures are not available from some other source, the second option is to use modified Newtonian pressures, i.e.

$$\frac{p}{p_s} = \left(1 - \frac{p_\infty}{p_s}\right)\cos^2\psi + \frac{p_\infty}{p_s} \tag{114}$$

where the angle ψ is given by eq. (78). Since derivatives of the pressure are needed to calculate the streamline geometry and scale factor, modified Newtonian pressure ratios are computed for each body coordinate used to generate the body geometry, and then the same pressure spline function described above is used to spline fit this data. In the "shadowed" region ($\cos\psi < 0$), $p = p_\infty$ is used.

Gas Properties at Edge of Boundary Layer

In the calculation of heating rates, the local pressure (p_e), density (ρ_e), enthalpy (h_e), velocity (U_e), speed of sound (a_e), and coefficient of viscosity (μ_e) are needed at the edge of the boundary layer. The first-order boundary-layer approximations allow the pressure at the edge of the boundary layer to be the same as the corresponding surface pressure ($p_e \approx p$), which was discussed in the previous section. Also, the boundary layer is assumed to remain sufficiently thin so that the entropy at the edge of the boundary layer is constant and equal to that value aft of a normal shock wave. This section describes how to calculate the other flow-field properties from the pressure and stagnation properties.

Equilibrium air properties. - Many elaborate computer programs are available for calculating equilibrium air properties. However, these more sophisticated approaches require considerable computational time and storage locations. In order to keep the computations relatively simple, the correlation formulas of Cohen (ref. 22) re used here to calculate the equilibrium air properties.

These formulas were shown to be quite accurate in ref. 22 for pressures in the range 10^{-4} atm. $\leq p \leq$ 10 atm. and an enthalpy range from 128.7 BTU/lb (corresponding to a temperature of 540°F) to 16,930 BTU/lb (corresponding to flight at approximately 29,000 ft/sec).

Assuming an isentropic expansion from the stagnation point, eq. (65) in ref. 17 gives the enthalpy (h_e) as

$$h_e = H_s \left\{ \frac{3.3454 \times 10^8}{h_E} \left[\frac{p_s}{2117}\right]^{.035} \left[\frac{(\frac{p}{p_s})^{.035} - 1}{(H_s/h_E)^{.3877}}\right] + 1 \right\}^{\frac{1}{.3877}} \qquad (115)$$

where H_s is the stagnation enthalpy and

$$h_E = 2.119 \times 10^8 \text{ ft}^2/\text{sec}^2$$

This approximate equation for h_e is more restrictive than the limitations given previously. Beckwith and Cohen (ref. 17) found that eq. (115) gave results generally within 3 percent of highly accurate computerized properties except when $p_s > 5$ atm with $H_s < 4{,}500$ BTU/lb.

With h_e given by eq. (115), the density can be computed from the equation (see ref. 22)

$$\rho_e = \frac{7.344 \times 10^{-5} \left(\frac{p}{2117}\right)^{.965}}{1 - 1.0477 \left[1 - \left(\frac{h_e}{h_E}\right)^{.6123}\right]} \qquad (116)$$

and then the coefficient of viscosity is

$$\mu_e = \frac{2.0144 \times 10^{-10} \left(\frac{p}{2117}\right)^{.992}}{\rho_e \left\{1 - 1.0213 \left[1 - \left(\frac{h_e}{h_E}\right)^{.3329}\right]\right\}} \qquad (117)$$

The velocity is obtained from the adiabatic energy equation as

$$U_e = [2(H_s - h_e)]^{1/2} \qquad (118)$$

Although the local speed of sound a_e is not given in ref. 22, it can be readily calculated as follows. Since the entropy at the edge of the boundary layer is assumed to be constant,

$$a_e^2 = \frac{dp}{d\rho_e} \qquad (119)$$

The inverse derivative $d\rho_e/dp$ can be obtained from the derivative of eq. (116), using the isentropic relation $dh_e = dp/\rho_e$. The result is

$$\frac{1}{a_e^2} = \frac{d\rho_e}{dp} = .965\,\frac{\rho_e}{p} - \frac{(.6415)\left[\frac{h_e}{h_E}\right]^{.6123}}{h_e\left\{1 - 1.0477\left[1 - \left(\frac{h_e}{h_E}\right)^{.6123}\right]\right\}} \qquad (120)$$

Finally, the Mach number follows from

$$M_e = \frac{U_e}{a_e} \qquad (121)$$

Perfect gas properties. - For a perfect gas with $\gamma = 1.4$, the usual isentropic relations, as given in ref. 27, may be used to obtain the following equations:

$$h_e = H_s\left[\frac{p}{p_s}\right]^{2/7} \qquad (122)$$

$$\rho_e = \rho_s\left[\frac{p}{p_s}\right]^{5/7} \qquad (123)$$

$$U_e = [2(H_s - h_e)]^{1/2} \qquad (124)$$

$$T_e = \frac{h_e}{6006} \qquad (125)$$

The coefficient of viscosity is computed from Sutherland's law, which gives

$$\mu_e = \frac{2.27 \times 10^{-8}\, T_e^{3/2}}{T_e + 198.6} \qquad (126)$$

and the speed of sound is simply

$$a_e^2 = (1.4)p/\rho_e \tag{127}$$

Stagnation properties. - In the analysis here the stagnation streamline is assumed to pass through the normal part of the bow shock wave. It is then necessary to calculate both equilibrium air and perfect gas stagnation-properties from known values of p_∞, ρ_∞, T_∞, and V_∞.

First, consider equilibrium air. The conservation equations for mass, momentum, and energy across a normal shock wave are:

$$\rho_\infty V_\infty = \rho_2 v_2 \tag{128}$$

$$p_\infty + \rho_\infty V_\infty^2 = p_2 + \rho_\infty V_\infty v_2 \tag{129}$$

$$H_s = h_\infty + \frac{V_\infty^2}{2} = h_2 + \frac{v_2^2}{2} \tag{130}$$

These equations must be solved iteratively for equilibrium air, and the procedure used here is as follows:

1. Assume $v_2 = 0$.
2. Calculate p_2 from eq. (129).
3. Calculate h_2 from eq. (130).
4. Calculate ρ_2 from eq. (116).
5. Compute a new value of v_2 from eq. (128); then go back to step 2 and start the process again.
6. Repeat steps 2 through 5 until the new value of v_2 is sufficiently close to its previous value to give convergence. For an accuracy of 10^{-5}, six iterations will generally suffice.

Using p_2, h_2, and H_s, eq. (115) can be rearranged to give

$$p_s = p_2 \left\{1 + \frac{h_E}{3.345 \times 10^8} \left[\frac{2117}{p_2}\right]^{.035} \left[\frac{h_2}{h_E}\right]^{.3877} \left[\left(\frac{H_s}{h_2}\right)^{.3877} - 1\right]\right\}^{\frac{1}{.035}} \tag{131}$$

then eq. (116) can be used to calculate ρ_s.

For a perfect gas with $\gamma = 1.4$, ref. 27 gives the stagnation pressure density as

$$p_s = p_\infty (1.2\, M_\infty^2)^{3.5} \left[\frac{7.2\, M_\infty^2}{7\, M_\infty^2 - 1} \right]^{2.5} \tag{132}$$

$$\rho_s = \rho_\infty \frac{6\, M_\infty^2}{(M_\infty^2 + 5)} \left[\frac{7.2\, M_\infty^2}{7\, M_\infty^2 - 1} \right]^{2.5} \tag{133}$$

Stagnation- Point Heat-Transfer Rate

For general three-dimensional stagnation points, the correct limiting form of the stagnation-point heat-transfer rate through the use of the axisymmetric analogue was not possible in analyses such as references 5, 11, and 26 because an accurate evaluation of the scale factor h could not be obtained in the stagnation region. The correct limiting form of the stagnation-point heat-transfer rate can be obtained in the present analysis since eq. (104) gives an accurate expression for scale factor h in the stagnation region. To prove this assertion, it will be shown that when the axisymmetric analogue is applied to Lees' method (ref. 16) for computing q_w, the limiting form at the stagnation point is the same as the general three-dimensional stagnation-point heat-transfer rate obtained by Reshotko (ref. 25) for a cold wall*.

In the application of the axisymmetric analogue, the heating rate along an inviscid surface streamline is obtained from the expression for the heating rate on an equivalent body of revolution at zero angle-of-attack when the body radius is replaced by the scale factor h and the distance along the surface of the body of revolution is replaced by the distance along the inviscid surface streamline. With these replacements, Lees' equation for a cold wall (ref. 16) becomes

$$q_w = \frac{0.5\, Pr^{-.67} \sqrt{\rho_e \mu_e V_\infty}}{778 \sqrt{2}} \; \frac{H_s \frac{p}{p_s} \frac{U_e}{V_\infty} h}{\left[\int_0^s \frac{p}{p_s} \frac{U_e}{V_\infty} h^2\, DS \right]^{1/2}} \tag{134}$$

* The axisymmetric analogue, or small cross flow assumption, was not used in Reshotko's analysis.

where the factor 778 has been added to make q_w have the dimensions of BTU/ft^2-sec. This equation can be applied independently to any inviscid surface streamline. However, it becomes indeterminate at the stagnation point since both U_e and h go to zero there. This indetermancy can be resolved by the use of the results obtained in the section on Stagnation Region Streamlines.

From eq. (104), the scale factor h in the stagnation region is

$$h = \frac{(\sin^2\beta + B\cos^2\beta)\ S_T}{G\sin\beta} \tag{135}$$

where

$$G \equiv [B^2\cos^2\beta + \sin^{2B}\beta\ (S_T/\varepsilon)^{2-2B}]^{1/2} \tag{136}$$

Replacing V by the velocity at the edge of the boundary layer U_e, eqs. (91) and (93) may be combined to give

$$U_e = V = \frac{V_T}{\sin\theta} = \frac{G\ S_T\ (\partial V_T/\partial S_T)_s}{\sin^B\beta\ (S_T/\varepsilon)^{1-B}} \tag{137}$$

and also

$$DS = \frac{DS_T}{\sin\theta} = \frac{G\ DS_T}{\sin^B\beta\ (S_T/\varepsilon)^{1-B}} \tag{138}$$

These equations are accurate to the first order in the stagnation region, and to be consistent the pressure ratio to first order of accuracy is

$$\frac{p}{p_s} = 1 \tag{139}$$

Eqs. (135) through (139) can now be used to evaluate the integral in eq. (134) as

$$\int_0^s \frac{p}{p_s}\frac{U_e}{V_\infty}\ h^2\ DS = \frac{1}{V_\infty}\left[\frac{\partial V_T}{\partial S_T}\right]_s \frac{(\sin^2\beta + B\cos^2\beta)^2\ \varepsilon^{2-2B}\ S_T^{\ 2+2B}}{\sin^{2+2B}\beta\ (2+2B)} \tag{140}$$

which can be used to evaluate the indeterminate part of eq. (134) as follows:

$$\lim_{s\to 0} \frac{\frac{p}{p_s}\frac{U_e}{V_\infty} h}{\left[\int_0^s \frac{p}{p_s}\frac{U_e}{V_\infty} h^2 \, DS\right]^{1/2}} = \left[\frac{1}{V_\infty}\left[\frac{V_T}{S_T}\right]_s 2(1+B)\right]^{1/2} \tag{141}$$

Using this result, the limiting form of eq. (134) becomes

$$q_{w,s} = \frac{0.5}{778}\sqrt{1+B}\,Pr^{-.67}\,H_s\sqrt{(\rho_e\,\mu_e)_s\left[\frac{\partial V_T}{\partial S_T}\right]_s} \tag{142}$$

Consistent with Lees' approximations for a cold wall, $H_s \approx H_s - h_w$, $(\rho_e\,\mu_e)_s \approx (\rho_w\,\mu_w)_s$, and thus eq. (142) is essentially the same as Reshotko's equation (ref. 25).

For the present analysis eq. (142) is modified so that it will reduce to two-dimensional and axisymmetric stagnation-point heat-transfer rates that are compatible with experimental results. In ref. 17 the following equations were found to compare reasonably well with experimental data:

$$(q_{w,s})_{2-D} = \frac{0.577}{778}\,Pr^{-.6}\,(\rho_e\,\mu_e)_s^{.44}\,(\rho_w\,\mu_w)_s^{.06}\sqrt{\left[\frac{DU_e}{DS}\right]_s}\,(H_s - h_w) \tag{143}$$

$$(q_{w,s})_{axisym.} = \frac{0.768}{778}\,Pr^{-.6}\,(\rho_e\mu_e)_s^{.4}\,(\rho_w\mu_w)_s^{.1}\sqrt{\left[\frac{DU_e}{DS}\right]_s}\,(H_s - h_w) \tag{144}$$

Consistent with the analysis of ref. 26, the factors 0.577 and 0.768 in eqs. (143) and (144), respectively, are replaced by

$$0.768\sqrt{\frac{1+B}{2}}\;\frac{\zeta_w'(\bar\beta_s)}{\zeta_w'(\bar\beta_s = .5)} \tag{145}$$

for the general three-dimensional stagnation point. Using the axisymmetric analogue, the pressure-gradient parameter $\bar\beta$ for a relatively cool and isothermal wall is determined from eq. (33) in ref. 17 as

$$\frac{\bar{\beta}\, t_e}{\frac{D}{DS}\left[\frac{U_e}{V_\infty}\right]} = \frac{2\int_0^s \frac{p}{p_s}\frac{U_e}{V_\infty} h^2\, DS}{\frac{p}{p_s}\left[\frac{U_e}{V_\infty} h\right]^2} \tag{146}$$

where $t_e = h_e/H_s$. For a sphere $\bar{\beta}_s = 0.5$, whereas $\bar{\beta}_s = 1$ for a cylinder. Using eqs. (146) and (135) through (139), it is found that $\bar{\beta}_s$ for a general three-dimensional stagnation point is

$$\left.\begin{aligned} \bar{\beta}_s &= \frac{1}{B+1} \qquad \text{for} \qquad B > 1 \\ \text{and} \qquad \bar{\beta}_s &= \frac{B}{B+1} \qquad \text{for} \qquad 0 \le B \le 1 \end{aligned}\right\} \tag{147}$$

However, Beckwith (ref. 5) found that $\bar{\beta}_s \approx 1 - \frac{B}{2}$ for $.5 \le B \le 1$, which gives the correct limiting values for a sphere ($B = 1$, $\bar{\beta}_s = \frac{1}{2}$) and a cylinder ($B = 0$, $\bar{\beta}_s = 1$) but disagrees with eq. (147) above. Eq. (147) gives $\bar{\beta}_s = \frac{1}{2}$ for a sphere ($B = 1$), but for the cylinder ($B = 0$) it gives $\bar{\beta}_s = 0$. This result is not surprising for the axisymmetric analogue because the streamlines are assumed to originate from a single stagnation point, and therefore all the streamlines on the cylinder are forced to emanate from this stagnation point rather than from the stagnation line along a generator of the cylinder. As will be shown below, the pressure-gradient parameter $\bar{\beta}_s$ has only a small influence on the magnitude of the term given by eq. (145).

From eqs. (52) and (59) in ref. 26, the following equation is obtained

$$\frac{\zeta_w'(\bar{\beta}_s)}{\zeta_w'(\bar{\beta}_s = .5)} = 1.033\left[\frac{1 + .527\,\bar{\beta}_s^{\,.686}}{1.116 + .411\,\bar{\beta}_s^{\,.686}}\right] \tag{148}$$

Using this result in eq. (145), the modified form of eq. (142) consistent with eqs. (143) and (144) is

$$q_{w,s} = \frac{.768}{778}\sqrt{\frac{B+1}{2}}\ (1.033)\left[\frac{1 + .527\ \bar{\beta}_s^{\ .686}}{1.116 + .411\ \bar{\beta}_s^{\ .686}}\right] Pr^{-.6}\sqrt{\left[\frac{\partial V_T}{\partial S_T}\right]_s}$$

$$\times\ (\rho_w\ \mu_w)_s^{\ a}\ (\rho_e\ \mu_e)_s^{\ b}\ (H_s - h_w) \qquad (149)$$

The exponents a and b are assumed to vary linearily with $\bar{\beta}_s$ between the values for a sphere and a cylinder in eqs. (143) and (144). Hence,

$$a = 0.1 - (.08)(\bar{\beta}_s - .5) \qquad (150)$$

$$b = 0.5 - a \qquad (151)$$

The effect of $\bar{\beta}_s$ on $q_{w,s}$ is small since it enters eq. (149) primarily through the factor given by eq. (145), and this factor is only weakly dependent on $\bar{\beta}_s$, varying from .9256 for $\bar{\beta}_s = 0$ to 1.033 for $\bar{\beta}_s = 1$. The factor $\left[\frac{\partial V_T}{\partial S_T}\right]_s$ in eq. (149) is obtained from the modified Newtonian pressure distribution as

$$\left[\frac{\partial V_T}{\partial S_T}\right]_s = \frac{1}{R_T}\left[\frac{\partial V_T}{\partial \psi}\right]_s = \frac{1}{R_T}\sqrt{\frac{2(p_s - p_\infty)}{\rho_s}} \qquad (152)$$

Laminar Heat-Transfer Rates

Application of the axisymmetric analogue to solutions of the locally similar boundary-layer equations in ref. 26 gives the laminar heating-rate as

$$\frac{q_w}{q_{w,s}} = \left\{\frac{\rho_w \mu_w}{\left[\rho_w \mu_w\right]_s}\left[\frac{\bar{\beta}\ t_e}{\frac{D}{DS}\left(\frac{U_e}{V_\infty}\right)}\right]_s \frac{\frac{D}{DS}\left(\frac{U_e}{V_\infty}\right)}{\bar{\beta}\ t_e}\right\}^{1/2} \frac{\zeta_w'}{\zeta_{w,s}'} \qquad (153)$$

For a relatively cool wall the equation of state gives

$$\rho_w = \frac{p}{\bar{R}\ T_w} \tag{154}$$

Then for an isothermal wall and $\mu_w = \mu_w(T_w)$, it follows that

$$\frac{\rho_w \mu_w}{(\rho_w \mu_w)_s} = \frac{p}{p_s} \tag{155}$$

By substituting eq. (141) into (146), the following equation results.

$$\left[\frac{\bar{\beta}\ t_e}{\frac{D}{DS}\left(\frac{U_e}{V_\infty}\right)}\right]_s = \left[\frac{1}{V_\infty}\left[\frac{\partial V_T}{\partial \bar{S}_T}\right]_s (B+1)\right]^{-1} \tag{156}$$

The factor $\zeta_w'/\zeta_{w,s}'$ in eq. (153) is obtained from eq. (61) in ref. 26 as

$$\frac{\zeta_w'}{\zeta_{w,s}'} = \left[\frac{1.116 + .411\ \bar{\beta}_s^{\ .686}}{1 + .527\ \bar{\beta}_s^{\ .686}}\right]\left[\frac{1 + .527\ \bar{\beta}^{.686}}{1.116 + .411\ \bar{\beta}^{.686}}\right](1.1 - .1625t_e + .0625t_e^2)$$

$$\times \frac{(.85 + .15t_e - \zeta_w)}{(1 - \zeta_{w,s})} \tag{157}$$

As suggested by Cohen (page 33 of ref. 26), the first factor on the right side of eq. (157) was used to replace the factor 1.033^j in eq. (61) of ref. 26. Since the wall is assumed to be relatively cool and isothermal,

$$\zeta_w = \zeta_{w,s} = \frac{h_w}{H_s} \tag{158}$$

The final form of the laminar heating-rate ratio is obtained by substituting eqs. (146), (155), and (156) into eq. (153), which gives

$$\frac{q_w}{q_{w,s}} = \frac{\dfrac{p}{p_s}\,\dfrac{U_e}{V_\infty}\,h\,\dfrac{\zeta_w'}{\zeta_{w,s}'}}{\left[\dfrac{2(B+1)}{V_\infty}\,\left[\dfrac{\partial V_T}{\partial S_T}\right]_s \displaystyle\int_0^s \dfrac{p}{p_s}\,\dfrac{U_e}{V_\infty}\,h^2\,DS\right]^{1/2}} \tag{159}$$

where the factor $\zeta_w'/\zeta_{w,s}'$ is obtained from eq. (157), B is determined from eqs. (107) to (109), and $\left[\dfrac{\partial V_T}{\partial S_T}\right]_s$ may be obtained from the modified Newtonian value given by eq. (152).

Laminar heating rates are obtained by applying eq. (159) along an inviscid surface streamline from the stagnation region to the end of the body or the beginning of the transition region, whichever comes first. Heating rates along each streamline are computed independently of the other streamlines. The integral in the denominator of eq. (159) can be evaluated by quadrature for each integration step along a streamline.

Transition Region Heating Rates

The location of the transition region on a body is a subject open to much speculation and debate. It is not proposed that the present method will predict the location of the transition region. Instead, the beginning and end of the transition region may be specified by one of the three options listed below.

1. Geometric location, or
2. A specified value of the integrated unit Reynolds number along a surface inviscid streamline, i.e. $Rn_1 = \displaystyle\int_0^s \frac{\rho_e U_e}{\mu_e}\,DS$, or
3. A specified value of the momentum thickness Reynolds number, $Rn_m = \dfrac{\rho_e\,U_e\,\theta_m}{\mu_e}$, along the inviscid surface streamline.

Once the beginning and end of transition is determined by one of the three methods above, the heating rate in the transition region is calculated as a weighted average of the local laminar and turbulent heating rates. Thus the heating rate is written as

$$q_w = q_{w_{lam}} + w_f (q_{w_{turb}} - q_{w_{lam}}) \tag{160}$$

where w_f is the "weighting" function with $w_f = 0$ at the beginning of transition and $w_f = 1$ at the end of transition. A method for calculating the turbulent heating rates is given in the next section.

The "weighting" function w_f is determined by a method similar to that of Dhawan and Narasimha (ref. 18). This method uses a Gaussian distribution for w_f, given by

$$w_f = 1 - \exp(-.412\ \xi_{tr}^2) \tag{161}$$

where

$$\xi_{tr} = \frac{S - S_{tri}}{\lambda}\ , \tag{162}$$

S is distance along the inviscid surface streamline, S_{tri} is the distance along the streamline where transition begins, and S_{tre} is the distance where transition ends.

For a finite transition region, the parameter λ in eq. (162) would have to be zero if w_f were exactly one at the end of transition. Here, λ will be chosen such that $w_f = 1 - 10^{-4}$ at the end of the transition region, which was the value used by Harris in ref. 2. The expression for λ which satisfies this condition is

$$\lambda = \frac{S_{tre} - S_{tri}}{4.74} \tag{163}$$

Then eq. (161) gives the "weighting" function as

$$w_f = 1 - \exp\left\{ -.412 \left[\frac{4.74\ (S - S_{tri})}{(S_{tre} - S_{tri})} \right]^2 \right\} \tag{164}$$

The equation above can be easily applied for those cases where the beginning and end of the transition region is specified by geometric location on the body. If the coordinates of several points on the boundary of the transition region are known, a one-dimensional cubic spline can be fit to this data to determine the axial location of the beginning and end of transition for any circumferential position.

However, when transition is specified by the integrated unit Reynolds number or momentum thickenss Reynolds number, the corresponding geometric position along a streamline for the end of transition may lie off the body surface. In this situation the value of S_{tre} cannot be determined. To circumvent this situation, the "weighting" function for these two options will be based on the value of the integrated unit Reynolds number (Rn_1) or momentum thickness Reynolds number (Rn_m). Therefore eq. (164) becomes

$$w_f = 1 - \exp\left\{ -.412 \left[\frac{4.74\ (R_{n_1} - R_{n_1,tri})}{(R_{n_1,tre} - R_{n_1,tri})} \right]^2 \right\} \tag{165}$$

when transition is based on the integrated unit Reynolds number, or

$$w_f = 1 - \exp\left\{ -.412 \left[\frac{4.74\ (R_{n_m} - R_{n_m,tri})}{(R_{n_m,tre} - R_{n_m,tri})} \right]^2 \right\} \tag{166}$$

for transition based momentum thickness Reynolds number, where the subscript "tri" refers to the beginning of transition and "tre" refers to the end of transition.

Turbulent Heat-Transfer Rates

Cooke and Hall (ref. 6) have shown that the axisymmetric analogue is applicable to turbulent as well as laminar boundary layers. There are many methods that could be used to calculate turbulent heating rates on axisymmetric bodies. The approach used here is to apply the axisymmetric analogue to a modified form of the integral method of Reshotko and Tucker (ref. 20) to obtain the turbulent momentum thickness. Then the momentum thickness is used to calculate the local skin friction coefficient from the correlation formula of Spalding and Chi (ref. 19), and finally the Karman form of Reynolds Analogy (see ref. 21) is used to calculate the turbulent heating rate corresponding to the skin friction coefficient.

Momentum thickness. - Reshotko and Tucker (ref. 20) developed an integral method to calculate the momentum thickness from the numerical solution of two first-order differential equations for θ_m and H_i along a streamline for a perfect gas. This method is modified here to apply to a perfect gas or equilibrium air, and the skin friction coefficient used in the method is that value computed simultaneously from the Spalding-Chi approach described below.

The basic method used by ref. 20 can be applied to both perfect and equilibrium gases if the ratio $a_e/a_{e,s}$ is replaced by $\sqrt{h_e/H_s}$. For the perfect gas these two expressions are one and the same; however, they are different for an equilibirum gas. As a result, the quantity $\frac{1}{M_e}\frac{DM_e}{DS}$ must be replaced by $\frac{H_s}{h_eU_e}\frac{DU_e}{DS}$. Then the integral form of the momentum equation becomes

$$\frac{D\theta_m}{DS} + (2 + H - M_e^2)\frac{\theta_m}{U_e}\frac{DU_e}{DS} + \frac{\theta_m}{h}\frac{Dh}{DS} = \frac{C_f}{2} \quad (167)$$

where C_f is the local skin friction coefficient. Following ref. 20, the compressible form factor is given by

$$H \equiv \frac{\delta^*}{\theta_m} = \frac{H_s}{h_e}H_{tr} + \frac{U_e^2}{2h_e} \quad (168)$$

where

$$H_{tr} = H_i + (\frac{h_w}{H_s} - 1)(1.3) \quad (169)$$

The incompressible form factor H_i is calculated from the equation

$$\frac{DH_i}{DS} = -\frac{H_s}{h_eU_e}\frac{DU_e}{DS}\frac{H_i}{2}(H_i + 1)\left[(H_i^2 - 1) + (\frac{h_w}{H_s} - 1)\right.$$

$$\left.[2.6\ (H_i - 1) - \frac{.15}{4.3}(H_i + 1)^2]\right] - .03H_i\ (H_i - 1)\frac{C_f}{2\ \theta_m} \quad (170)$$

where due account has been made for a perfect gas or equilibrium air.

Eqs. (167) and (170) are integrated numerically along an inviscid surface streamline, starting at the beginning of the transition region. The initial values of θ_m and H are the laminar values given by ref. 17, and C_f is supplied by the Spalding-Chi approach described below.

Skin friction coefficient. - The turbulent skin-friction coefficient is determined by the correlation formula of Spalding and Chi (ref. 19) based on momentum thickness Reynolds number but modified to account for perfect or equilibrium gases. Eq. (52) of ref. 19 is modified to read

$$F_{R\delta} = (h_w/h_e)^{-.702}\,(h_{aw}/h_w)^{.772} \qquad (171)$$

where

$$\frac{h_{aw}}{h_e} = 1 + 0.89\,\frac{U_e^2}{2h_e} \qquad (172)$$

and the factor 0.89 is the turbulent recovery factor. With the definitions

$$R_\delta = \frac{\rho_e\,U_e\,\theta_m}{\mu_e} \qquad (173)$$

$$U_G^+ = (2/C_f\,F_c)^{1/2} \qquad (174)$$

the compressible form of eq. (28) in ref. 19 becomes

$$F_{R\delta}\,R_\delta = \frac{1}{6}\,(U_G^+)^2 + (KE)^{-1}\Big[\,[1 - (2/KU_G^+)]\exp(KU_G^+)$$

$$+ (2/KU_G^+) + 1 - \frac{1}{6}\,(KU_G^+)^2 - \frac{1}{12}\,(KU_G^+)^3$$

$$- \frac{1}{40}\,(KU_G^+)^4 - \frac{1}{180}\,(KU_G^+)^5\Big] \qquad (175)$$

where K = 0.4 and E = 12. In the application of eq. (175), $F_{R\delta}$ and R_δ are computed from eqs. (171) and (173), respectively, with θ_m obtained from the Reshotko-Tucker method described above. The U_G^+ is calculated from eq. (175) by an iterative scheme such as the Newton-Rhapson method. Using U_G^+, eq. (174) gives the incompressible skin friction coefficient since

$$C_{f,i} = F_c\,C_f \qquad (176)$$

Finally, C_f follows from eq. (176) once F_c has been evaluated.

In ref. 19, F_c is defined by

$$F_c = \left[\int_0^1 \left(\frac{\rho}{\rho_e}\right)^{1/2} d\left(\frac{U}{U_e}\right)\right]^{-2} \qquad (177)$$

where ρ and U are the density and velocity across the turbulent boundary layer. The boundary layer approximations give $p \approx p_e$, and for the perfect gas the equation of state yields

$$\frac{\rho}{\rho_e} = \frac{T_e}{T} = \frac{h_e}{h_{bl}} \tag{178}$$

where h_{bl} is the enthalpy inside the boundary layer, which is assumed to follow Crocco's relation

$$\frac{h_{bl}}{h_e} = \frac{h_w}{h_e} + \left[\frac{h_{aw} - h_w}{h_e}\right] \frac{U}{U_e} + \left[1 - \frac{h_{aw}}{h_e}\right] \frac{U^2}{U_e^2} \tag{179}$$

Upon substituting eqs. (178) and (179) into (177), the resulting expression can be integrated for the perfect gas to yield

$$F_c = \left[\frac{h_{aw}}{h_e} - 1\right] \left\{ \tan^{-1} \left[\frac{2\left[\frac{h_{aw}}{h_e} - 1\right] - \left[\frac{h_{aw} - h_w}{h_e}\right]}{2\sqrt{\frac{h_{aw}}{h_e} - 1}}\right] + \tan^{-1}\left[\frac{\left[\frac{h_{aw} - h_w}{h_e}\right]}{2\sqrt{\frac{h_w}{h_e}\left[\frac{h_{aw}}{h_e} - 1\right]}}\right] \right\}^{-2} \tag{180}$$

For equilibrium air eq. (180) is not valid because eq. (178) is based on a perfect gas. The density-enthalpy relation for equilibrium air is obtained from eq. (116) as

$$\frac{\rho}{\rho_e} = \frac{1 - 1.0477\,[1 - (h_e/h_E)^{.6123}]}{1 - 1.0477\,[1 - (h_e/h_E)^{.6123}\,(h_{bl}/h_e)^{.6123}]} \tag{181}$$

Then using eq. (179) in (181), the integral in eq. (177) is evaluated numerically to obtain F_c for equilibrium air.

Turbulent Heating-Rate Expression. - The Karman form of the Reynolds analogy factor is given by ref. 21 as

OF

36186

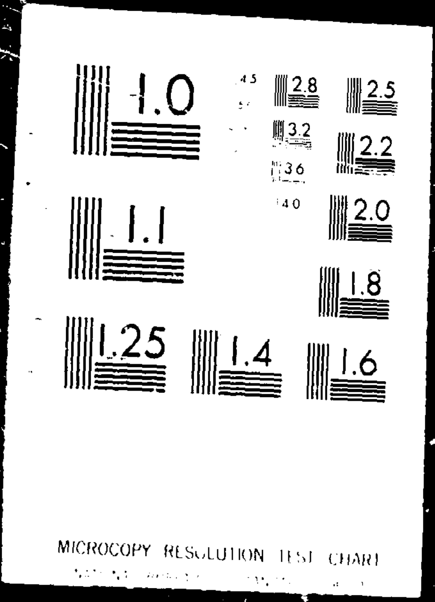
1.0
1.1
1.25
1.4
1.6
1.8
2.0
2.2
2.5
2.8
3.2
3.6
4.0
4.5
MICROCOPY RESOLUTION TEST CHART

$$2\frac{N_{ST,i}}{C_{f,i}} = \left\{1 + 5\sqrt{\frac{C_{f,i}}{2}}\left[Pr - 1 + \ln\left(\frac{5\,Pr + 1}{6}\right)\right]\right\}^{-1} \qquad (182)$$

where Pr = 0.725 was used. As in ref. 21, it is assumed that the compressible Reynolds analogy factor is the same as the incompressible factor, i.e.

$$2\frac{N_{ST}}{C_f} = 2\frac{N_{ST,i}}{C_{f,i}} \qquad (183)$$

Then, since

$$N_{ST} = \frac{q_w(778)}{\rho_e U_e (h_{aw} - h_w)} \qquad (184)$$

the turbulent heating rate follows from eqs. (182)-(184) as

$$q_{w_{turb}} = \frac{(h_{aw}-h_w)}{778}\,\rho_e U_e \frac{C_f}{2}\left\{1 + 5\sqrt{\frac{C_{f,i}}{2}}\left[Pr - 1 + \ln\left(\frac{5\,Pr+1}{6}\right)\right]\right\}^{-1}$$

(185)

Both C_f and $C_{f,i}$ are obtained from the Spalding-Chi approach described above.

COMPUTATIONAL METHOD

The method developed herein was programmed on the IBM 360/75 digital computer at the North Carolina State University. This program is also compatible with the CDC 6600 computer at the Langley Research Center, NASA. A detailed description of the computer program appears in Part II of this report (NASA CR-111922).

To run a typical case, the following data are needed as input parameters:

1. p_∞, T_∞, V_∞, α, ζ_w.
2. specify a perfect gas (γ = 1.4) or equilibrium air.
3. body geometry data as Cartesian coordinates of points around the circumference at several axial stations.
4. specify surface pressure distribution by one of the following three methods:

2 ⊕

a) p/p_s from some other source for points around the circumference at several axial stations along the body, or

b) modified Newtonian pressure distribution, or

c) modified Newtonian pressure distribution, but streamlines computed by the simplified method of ref. 14.

5. specify the beginning and end of the transition region by one of the following three methods:

   a) geometric location, which is specified by the Cartesian coordinates of points around the circumference of the body for both the beginning and end of transition, or

   b) values of Rn_m at the beginning and end of transition, or

   c) values of Rn_1 at the beginning and end of transition.

   If transitional and turbulent heating rates are not required, laminar heating rates alone may be calculated.

6. The value of β for each inviscid surface streamline to be computed, where $0 \leq \beta \leq 180°$, $\beta = 0$ is the streamline in the windward plane and $\beta = 180°$ is the streamline in the leeward plane.

All the input data used to calculate the results in this part of the report are given in Part II. The computer program calculates heating rates and other pertient data along each inviscid surface streamline independently of the other streamlines.

RESULTS

To illustrate the present method, results are presented for blunted cones at angles of attack, a blunted 70° slab delta wing, and the HL-10 lifting body.

Blunted Cones

Blunted 9° half-angle cone. - Figure 7 shows three inviscid surface streamlines ($\beta = 5°$, 20°, and 90°) calculated for a blunted 9° half-angle cone at $\alpha = 10°$ and $M_\infty = 18$ using a perfect gas ($\gamma = 1.4$). Each of the three streamlines was calculated by three different methods: (1) method of characteristics (ref. 28), (2) present method using modified Newtonian pressures, and (3) simplified streamlines by the method of reference 14. Although the geometry of this body could be represented by simple analytical expressions, the coordinates of 19 points around the circumference of the half body at 20 axial stations were used to generate the body geometry by the doubly cubic spline function. Figure 7 shows that the $\beta = 5°$ and 20° streamlines calculated by the present method using modified Newtonian pressures are in good agreement with the "exact" streamlines calculated by the method of characteristics. The $\beta = 90°$ streamline calculated by the present method does not agree well with the "exact" result, but this is to be expected since this streamline goes into the "shadowed" region ($\phi \geq 154°$) on the conical afterbody where the pressure is set equal to free-stream static pressure. The simplified streamlines are significantly lower than those calculated by the other two methods.

Blunted 15° half-angle cone. - In reference 29 Cleary gives tabulated experimental laminar heating-rates on a spherically blunted 15° half-angle cone at $M_\infty = 10.6$. In order to compare results from the present method with some of this data, streamlines and laminar heating rates were calculated on this configuration for $\alpha = 20°$, $R_o = 0.375''$, $p_\infty = 2.6614$ lb/ft^2, $T_\infty = 89.971°$R, and $V_\infty = 4928.1$ ft/sec, ($M_\infty = 10.6$). Although a perfect gas with $\gamma = 1.4$ was used in the calculations, gas imperfections in the wind tunnel stagnation properties of $p_s = 1.73 \times 10^5$ lb/ft^2 and $T_s = 2000°$R were taken into account to determine the free-stream conditions. In addition, it was determined that a value of $\zeta_w \equiv h_w/H_s = 0.251$ corresponds to $T_w/T_s = 0.270$.

The body geometry was specified by the coordinates of 20 points around the circumference of the half body at 19 axial stations. Streamline patterns, calculated by the present method using modified Newtonian pressures and by the simplified method of ref. 14, are shown in figure 8 for $\beta = 1°$, 10°, 15° and 45°. This figure shows that the streamlines move from the windward plane and rapidly approach the leeward plane, and the streamlines calculated by modified Newtonian pressures wrap around the surface at a steeper rate than the simplified streamlines. The "equivalent radius" or scale factor increases along a streamline on the windward side, where the streamlines are diverging, but decreases along the leeward side due to converging streamlines. As mentioned previously, the streamlines are continued into the "shadowed" region of the body ($\phi \geq 137.4°$), although the pressure is assumed to be free-stream static pressure in that region. It is possible that the flow separates from the surface somewhere in this region, and therefore the calculated streamlines and heating rates are questionable there.

Laminar heating-rate ratios ($q_w/q_{w,s}$), calculated by the present method using both the streamlines computed from modified Newtonian pressures and the simplified streamlines, are compared with Cleary's experimental data* in figures 9, 10, and 11. Figure 9 shows the heating-rate ratio along the windward plane, whereas figures 10 and 11 show the circumferential distribution of heating-rate ratios at axial stations of x = 3.56" and 9.36", respectively (corresponding to x_s/L = 0.207 and 0.466 in ref. 29). Very good agreement with the experimental data is obtained for the heating-rate ratios using modified Newtonian pressures and reasonably good agreement using simplified streamlines for this case. For this relatively simple body shape, the heating-rate ratios calculated using the simplified streamlines are close to those using modified Newtonian pressures although the streamlines themselves differ by a large amount (see fig. 8). It is significant to note that the ratio of the angle-of-attack to the cone half-angle is 1.33 for this case, and thus the present method is not limited to small angles of attack.

Blunted 70° Slab Delta Wing

This configuration is a 70° swept delta wing with a cylindrical leading edge which is tangent to a flat slab on the upper and lower surfaces. The blunt nose is a spherical cap, and the radius of both the spherical cap and cylindrical leading edge is one foot. Although this configuration could also be specified analytically, coordinates of 13 points around the semi-periphery at 19 axial stations ($0 \le x \le 1.95$ ft) were used to generate the body shape.

Figure 12 illustrates the streamline patterns calculated by the present method (using modified Newtonian pressures and a perfect gas) on this delta wing at $\alpha = 10°$ and $M_\infty = 8$ ($p_\infty = 10^3$ lb/ft^2, $T_\infty = 416°$R, $V_\infty = 8000$ ft/sec, and $\zeta_w = 0.4$). It can be seen that the $\beta = 10°$ streamline is converging towards the center line on the flat slab which causes the scale factor to start

---

* The experimental heating rates in ref. 29 are ratioed to the calculated $q_{w,s}$ = 35.94 BTU/ft^2-sec in this report.

decreasing. On the other hand, the $\beta = 60°$ streamline runs nearly parallel to the leading edge beyond the nose, and at $x = 2$ ft the scale factor is still increasing which indicates the streamlines in this region are diverging. The streamline patterns in figure 12 are qualitatively similar to the experimental oil-flow patterns in reference 30 for this angle of attack.

Laminar, transitional, and turbulent heating-rate ratios along the windward streamline ($\phi = 0$) are shown in figure 13. Transition was arbitrarily chosen to begin at $Rn_m = 10^3$ and end at $Rn_m = 2 \times 10^3$. These values were used to illustrate the capability of the present method to calculate transitional and turbulent heating rates, and they should not be construed to represent the actual transition region on this body. As shown in figure 13, the transition region corresponding to these values of Rn_m lies in the narrow band $0.268 \text{ ft} \leq x \leq 0.318$ ft. This figure also shows that the heating-rate ratio increases sharply in the transition region, and then decreases in the fully turbulent region. For $x \geq 1$ ft the windward streamline is on the flat slab where the heating-rate ratio decreases very slowly.

HL-10 Lifting Body

The geometry of the HL-10 lifting body without fins is illustrated by plan and side views in figure 14 and cross sections in figure 15. This body is an example of a shape whose geometry is difficult to describe analytically. In the present method the body geometry was generated from the coordinates of 20 points around the semi-periphery at 20 axial stations.

Figure 16 depicts laminar, transitional, and turbulent heating-rate ratios calculated along the center line of the lower surface for $\alpha = 20°$, $M_\infty = 10$, $p_\infty = 10^3$ lb/ft^2, $T_\infty = 416°R$, $V_\infty = 10^5$ ft/sec, and $\zeta_w = 0.1$. Equilibrium air and simplified streamlines were used in these calculations, and transition was arbitrarily chosen to begin at $x = 33.07''$ and end at $x = 54.24''$. Again, the heating-rate ratio increases sharply in the transition region, and then begins to decrease near the end of that region.

Difficulties were encountered for this case when modified Newtonian pressures were used to calculate the inviscid surface streamlines. Along the windward streamline the scale factor went to zero, which indicates merging or crossing of streamlines and invalidates the heating-rate calculations. This difficulty can be traced to the fact that away from the nose the lower surface of the HL-10 body is flat in the z-direction, and modified Newtonian pressures are constant across a flat surface. As shown in the Appendix, this feature of modified Newtonian pressures generally produces questionable results.

DISCUSSION

In the calculation of inviscid surface streamlines and scale factors, first and second derivatives of both the body geometry and pressure are needed. The doubly cubic spline function was found to represent the geometry of the bodies considered herein satisfactorily. However, its accuracy is affected by the number and location of body positions used, and the spline function does not smooth out data points (although it does smooth derivatives). When pressure data from some other source are used in the present method, they should be smoothed before using them so that the pressure spline function will be accurate.

Inviscid surface streamlines calculated from modified Newtonian pressures compared well with those from the method of characteristics for a 9° half-angle cone at $\alpha = 10°$ and $M_\infty = 18$, except for the "shadowed" region. In the "shadowed" region on the leeward side, the pressure is assumed to be constant at p_∞, and thus the streamlines calculated in this region are inaccurate and follow geodesics of the surface (see ref. 7). In addition, the flow may separate from the surface somewhere in the "shadowed" region, which makes the results from the present method questionable there.

The present method was found to predict laminar heating rates very well on a blunted 15° half-angle cone at $\alpha = 20°$ and $M_\infty = 10.6$ using modified Newtonian pressures. Additional comparisons of the present theory with experimental data on other body shapes and for transitional and turbulent heating should be made to assess the accuracy of the theory more thoroughly.

Bodies with flat segments, like the blunted 70° slab delta wing and the HL-10 lifting body, present difficulties when inviscid surface streamlines are calculated using modified Newtonian pressures or simplified streamlines. On a flat segment, both the modified Newtonian pressure and the angle σ are constant, and consequently eq. (48) shows that the streamlines are straight (θ = constant), and the direction of each streamline is determined by its direction upon entering that flat segment. Since each streamline may have a different direction at the beginning of the flat segment, it is possible for the streamlines calculated from modified Newtonian pressures to cross over one another*. In addition, eq. (75) shows that $D^2h/DS^2 = 0$ along these calculated streamlines which means that the scale factor h is linearly increasing or decreasing along the streamline, depending on the value of Dh/DS at the beginning of the flat segment. In particular, if $Dh/DS < 0$ it is easy to see how h calculated by this approximate method may go to zero (as encountered on the HL-10 body) and even become negative. The scale factor along the windward streamline is discussed more thoroughly in the Appendix. On a flat segment the simplified streamlines are all parallel and the scale factor h along each streamline is constant and equal to the value the streamline had upon entering the flat segment. The difficulties encountered on flat segments with these two approximate methods for calculating inviscid surface streamlines can be circumvented by calculating the streamlines from an accurate pressure distribution.

In the present method the boundary layer is assumed to be sufficiently thin that the flow may be considered to be isentropic at the edge of the boundary layer. This assumption may be invalid away from the stagnation point on some body shapes due to the boundary layer "swallowing" the entropy layer. When this occurs, the entropy at the edge of the boundary layer could be significantly less than the entropy aft of a normal shock wave.

The computational time required to compute the examples given herein is highly dependent on the number of streamlines specified in the input data. Typical cases with six streamlines calculated from modified Newtonian pressures required less than 4 minutes on the IBM 360/75 computer for a perfect gas. When simplified streamlines were used, the computational time was reduced about 50%. On the other hand, the computational time was increased about 10% when equilibrium air was used in place of a perfect gas.

---

* Of course, it is physically impossible for one surface streamline to cross another.

CONCLUDING REMARKS

A method is developed for calculating inviscid surface streamlines and laminar, transitional, and turbulent heating rates on general blunt-nosed three-dimensional bodies at angles of attack in hypersonic flows. Relatively simple techniques are employed to keep the computational storage and run time down to small values (less than 4 minutes for a typical case on the IBM 360/75 computer).

Streamlines calculated from the modified Newtonian pressure distribution were found to compared favorably with those from the method of characteristics on the windward side of a blunted 9° half-angle cone at $\alpha = 10°$ and $M_\infty = 18$. Laminar heating rates calculated on a blunted 15° half-angle cone at $\alpha = 20°$ and $M_\infty = 10.6$ compared very well with experimental data.

Streamlines and laminar, transitional, and turbulent heating rates were calculated on a blunted 70° slab delta wing at $\alpha = 10°$ and $M_\infty = 8$, and on the HL-10 lifting body at $\alpha = 20°$ and $M_\infty = 10$. These bodies have some flat segments, and since the modified Newtonian pressure is constant over a flat surface, streamline patterns and corresponding heating rates calculated from modified Newtonian pressures are questionable. This difficulty can be circumvented by using an accurate surface pressure distribution in lieu of modified Newtonian pressures.

The relatively small amount of numerical computations required coupled with reasonably good accuracy, makes the present method attractive for engineering applications. Additional comparsions with experimental data on other body shapes and for transitional and turbulent heating are needed to assess the accuracy of this method more thoroughly.

Mechanical and Aerospace Engineering Department,
North Carolina State University,
Raleigh, North Carolina, August 25, 1971.

APPENDIX

Scale Factor Along Windward Streamline

Along the windward streamline $\phi = 0$, $\beta = 0$, and symmetry requirements dictate that $\theta = 0$, $\delta_\phi = 0$, $\partial V/\partial\phi = 0$, and $\frac{1}{h}\frac{\partial}{\partial\beta} = \frac{1}{f}\frac{\partial}{\partial\phi}$. Therefore, for this streamline

$$\left.\frac{1}{h}\frac{\partial\theta}{\partial\beta}\right|_{\phi=0} = \left.\frac{1}{f}\frac{\partial\theta}{\partial\phi}\right|_{\phi=0} = \left.\frac{1}{Vf}\frac{\partial}{\partial\phi}(V \sin\theta)\right|_{\phi=0} \tag{A1}$$

and

$$\left.\frac{\sin\Gamma}{h}\frac{\partial\sigma}{\partial\beta}\right|_{\phi=0} = \left.\frac{1}{R_\phi}\frac{Df}{DS}\right|_{\phi=0} \tag{A2}$$

where

$$\sin\Gamma\Big|_{\phi=0} = \left.\frac{Df}{DS}\right|_{\phi=0} \tag{A3}$$

and

$$R_\phi = \left[\frac{1}{f}\frac{\partial\sigma}{\partial\phi}\right]^{-1}_{\phi=0} \tag{A4}$$

is the body radius of curvature in a cross-sectional plane (x = constant) at $\phi = 0$. When eqs. (A1) and (A2) are substituted into eq. (64), there results

$$\left.\frac{1}{h}\frac{Dh}{DS}\right|_{\phi=0} = \left[\frac{1}{Vf}\frac{\partial}{\partial\phi}(V\sin\theta) + \frac{1}{R_\phi}\frac{Df}{DS}\right]_{\phi=0} \tag{A5}$$

This equation can be integrated to give the scale factor along the windward streamline only when the velocity-gradient term on the right side is known. For an axisymmetric body ($\sigma \equiv \phi$), $R_\phi = f$ and eq. (A5) reduces to eq. (B-11) in reference 11.

When only the surface pressure distribution is known, eq. (75) must be used in lieu of eq. (A5) to calculate h, and along the windward streamline it reduces to

$$\frac{1}{h}\frac{D^2h}{DS^2}\bigg|_{\phi=0} = -\frac{\cos\Gamma}{R_x R_\phi} + \frac{1}{\rho V^2}\left[\left(\frac{1}{h}\frac{Dh}{DS} - \frac{1}{R_\phi}\frac{Df}{DS}\right)\left(-\frac{Dp}{DS}\right) + \frac{1}{f^2}\frac{\partial^2 p}{\partial\phi^2}\right]\bigg|_{\phi=0} \tag{A6}$$

where

$R_x = -\dfrac{1}{\cos\Gamma\,\dfrac{\partial\Gamma}{\partial x}}$ is the body radius of curvature in the $\phi = 0$ plane. If the lower surface of a three-dimensional body is flat in the z-direction, then $R_\phi \to \infty$ and due to symmetry $(\partial p/\partial\phi)_{\phi=0} = 0$ but generally $(\partial^2 p/\partial\phi^2)_{\phi=0} \neq 0$, although the modified Newtonian pressure distribution gives $(\partial^2 p/\partial\phi^2)_{\phi=0} = 0$. When a segment of the lower surface is flat in two directions, then $R_\phi \to \infty$ and $R_x \to \infty$ and eq. (A6) reduces to

$$\frac{1}{h}\frac{D^2h}{DS^2}\bigg|_{\phi=0} = -\frac{1}{\rho V^2}\frac{1}{h}\frac{Dh}{DS}\frac{Dp}{DS} + \frac{1}{f^2}\frac{\partial^2 p}{\partial\phi^2}\bigg|_{\phi=0} \tag{A7}$$

This equation will yield the correct scale factor along the windward streamline on a flat segment only if the correct pressure distribution is used. When the modified Newtonian pressure distribution is used, eq. (A7) reduces to $(D^2h/DS^2)_{\phi=0} = 0$, which generally gives incorrect results on a flat segment.

REFERENCES

1. Inoyue, M.; Rakich, J. V.; and Lamax, H.: A Description of Numerical Methods and Computer Programs for Two-Dimensional and Axisymmetric Supersonic Flow Over Blunt-Nosed and Flared Bodies. NASA TN D-2970, 1965.

2. Harris, J. E.: Numerical Solution of the Compressible Laminar, Transitional, and Turbulent Boundary Layer Equations with Comparisons to Experimental Data. Ph.D. Dissertation, Virginia Polytechnic Institute, 1970.

3. Rakich, J. V.: A Method of Characteristics for Steady Three-Dimensional Supersonic Flow with Application to Inclined Bodies of Revolution. NASA TN D-5341, 1969.

4. Moretti, G.; and Abbett, M.: A Time-Dependent Computational Method for Blunt Body Flows. AIAA J., vol. 4, no. 12, Dec. 1966, pp. 2136-2141.

5. Beckwith, I. E.: Similarity Solutions for Small Cross Flows in Laminar Compressible Boundary Layers. NASA TR R-107, 1961.

6. Cooke, J. C.; and Hall, M. G.: Boundary Layers in Three Dimensions, Rep. No. Aero. 2635, British R. A. E., Feb. 1960.

7. Leigh, D. C.; and Ross, B. B.: Surface Geometry of Three-Dimensional Inviscid Hypersonic Flows. AIAA J., vol. 7, no. 1, Jan. 1969, pp. 123-129.

8. Maikapar, G. I.: Calculation of Streamlines with a Known Pressure Distribution on the Surface of a Rigid Body. J. of Appl. Math. and Mech., Jan. 1965, pp. 468-470 (Translated from PMM vol. 28, no. 2, 1964, pp. 381-382).

9. Timmer, H. G.: Determination of Hypersonic, Inviscid, Surface Streamlines for General Convex Bodies. Douglas Paper 10005, McDonnell Douglas Astronautics Co., Sept., 1969.

10. Pinkus, O.; and Cousin, S. B.: Three Dimensional Boundary Layers on Cones at Small Angles of Attack. Trans. ASME, ser. E., vol. 35, no. 4, Dec. 1968, pp. 634-640.

11. Vaglio-Laurin, R.: Laminar Heat Transfer on Three-Dimensional Blunt Nosed Bodies in Hypersonic Flow. Jet Propulsion (ARS J.), vol. 29, no. 2, Feb. 1959, pp. 123-129.

12. Pasiuk, L.: Comparisons of Experimental and Theoretical Heat Transfer to a Yawed Sphere-Cone Model at Supersonic Speeds. NOL TR 63-208, 1963.

13. Bushnell, D. M.; Jones, R. A.; and Huffman, J. K.: Heat-Transfer and Pressure Distributions on Spherically Blunted 25° Half-Angle Cone at Mach 8 and Angles of Attack Up to 90°. NASA TN D-4792, 1968.

14. DeJarnette, F. R.; and Davis, R. M.: A Simplified Method for Calculating Laminar Heat Transfer Over Bodies at an Angle of Attack. NASA TN D-4720, 1968.

15. DeJarnette, F. R.; and Tai, T. C.: A Method for Calculating Laminar and Turbulent Convective Heat Transfer Over Bodies at an Angle of Attack. NASA CR-101678, March, 1969.

16. Lees, L.: Laminar Heat Transfer Over Blunt-Nosed Bodies at Hypersonic Flight Speeds. Jet Propulsion (ARS J.), vol. 26, no. 4, Apr., 1956, pp. 259-269, 274.

17. Beckwith, I. E.; and Cohen, N. B.: Application of Similar Solutions to Calculation of Laminar Heat Transfer on Bodies with Yaw and Large Adverse Pressure Gradient in High-Speed Flow. NASA TN D-625, 1961.

18. Dhawan, S.; and Narasimha, R.: Some Properties of Boundary Layer Flow During the Transition from Laminar to Turbulent Motion. J. Fluid Mech., vol. 3, no. 4, Apr. 1958, pp. 418-436.

19. Spalding, D. B.; and Chi, S. W.: The Drag of a Compressible Turbulent Boundary Layer on a Smooth Flat Plate With and Without Heat Transfer. J. Fluid Mech., vol. 18, pt. 1, Jan. 1964, pp. 117-143.

20. Reshotko, E.; and Tucker, M.: Approximate Calculation of the Compressible Turbulent Boundary Layer with Heat Transfer and Arbitrary Pressure Gradient. NACA TN 4154, 1957.

21. Bertram, M. H.; and Neal, L.: Recent Experiments in Hypersonic Turbulent Boundary Layers. Paper presented at the AGARD Specialists Meeting on Recent Developments in Boundary-Layer Research, Sponsored by the Fluid Dynamics Panel of AGARD, Naples, Italy, 1965.

22. Cohen, N. B.: Correlation Formulas and Tables of Density and Some Transport Properties of Equilibrium Dissociating Air for Use in Solutions of the Boundary Layer Equations. NASA TN D-194, 1960.

23. Ahlberg, J. H.; Nilson, E. N.; and Walsh, J. L.: The Theory of Splines and Their Applications. Academic Press, 1967.

24. Weatherburn, C. E.: Differential Geometry of Three Dimensions. Vol. I, Cambridge at the University Press, 193..

25. Reshotko, E.: Heat Transfer to a General Three-Dimensional Stagnation Point. Jet Propulsion (ARS J.), vol. 28, no. 1, Jan. 1958, pp. 58-60.

26. Cohen, N. B.: Boundary-Layer Similar Solutions and Correlation Equations for Laminar Heat-Transfer Distribution in Equilibrium Air at Velocities Up to 41,100 Feet Per Second. NASA TR R-118, 1961.

27. Ames Research Staff: Equations, Tables and Charts for Compressible Flow. NACA Rept. 1135, 1953.

28. Knox, E. C.; and Lewis, C. H.: A Comparison of Experimental and Theoretically Predicted Pressure Distributions and Force and Stability Coefficients for a Spherically Blunted Cone at $M_\infty = 18$ and Angle of Attack. AEDC TR-65-234, Feb. 1966.

29. Cleary, J. W.: Effects of Angle of Attack and Bluntness on Laminar Heating-Rate Distributions of a 15° Cone at a Mach Number of 10.6. NASA TN D-5450, 1969.

30. Bertram, M. H.; and Everhart, P. E.: An Experimental Study of the Pressure and Heat-Transfer Distribution on a 70° Sweep Slab Delta Wing in Hypersonic Flow. NASA TR R-153, 1963.

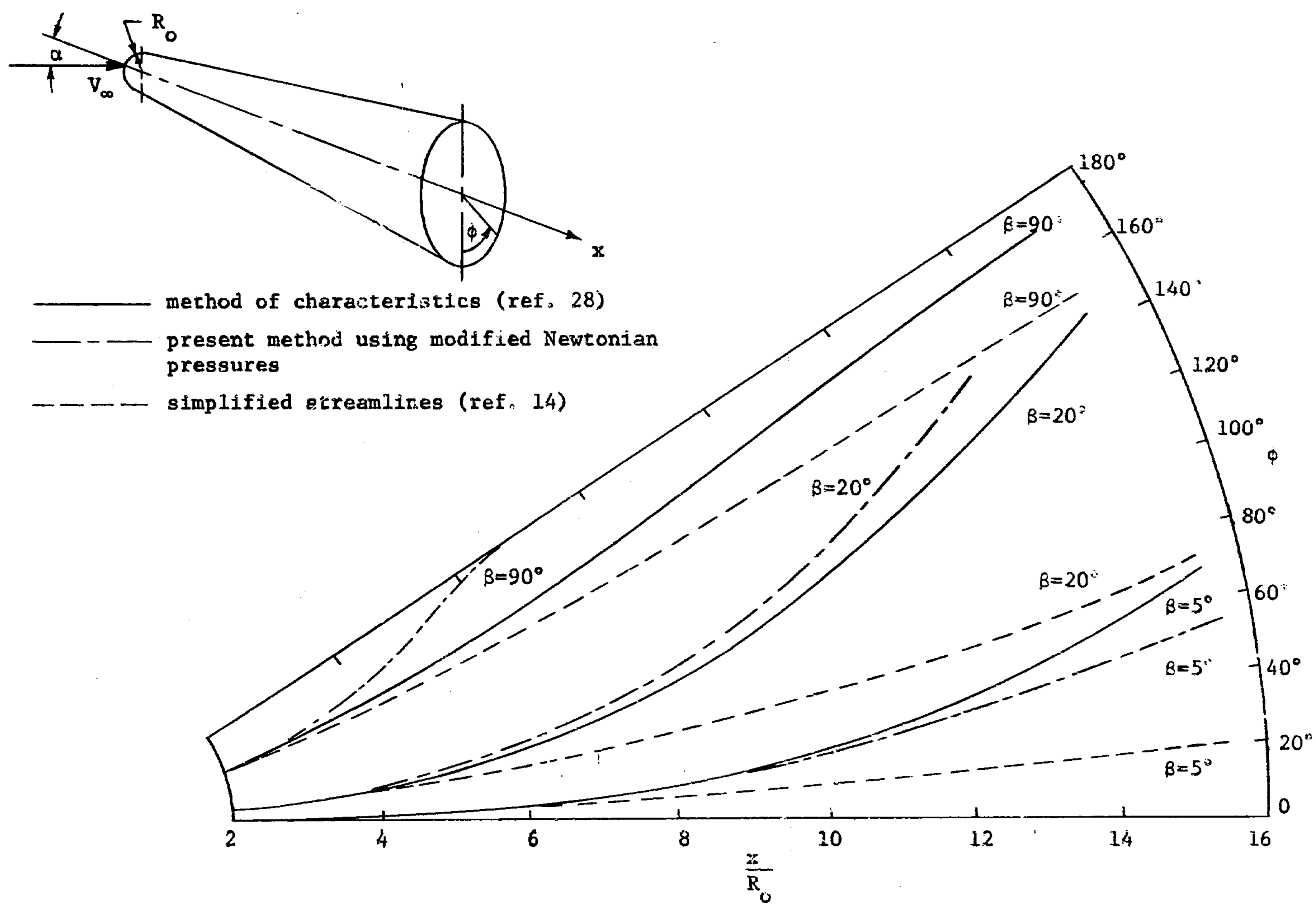

Figure 7. Streamlines on a blunted 9° half-angle cone at $\alpha = 10°$ and $M_\infty = 18$

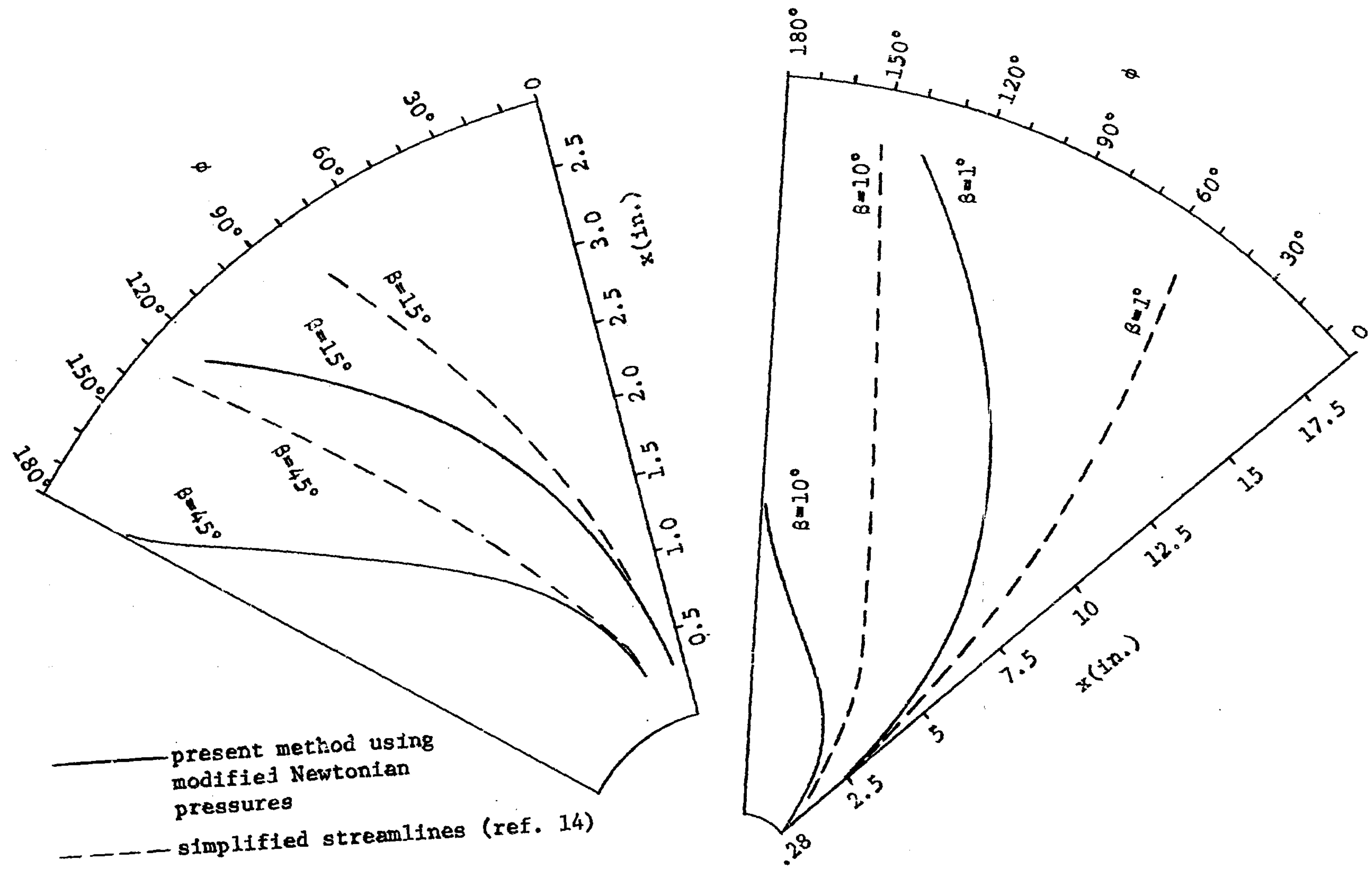

Figure 8. Streamlines on blunted 15° half-angle cone at $\alpha = 20°$ and $M_\infty = 10.6$.

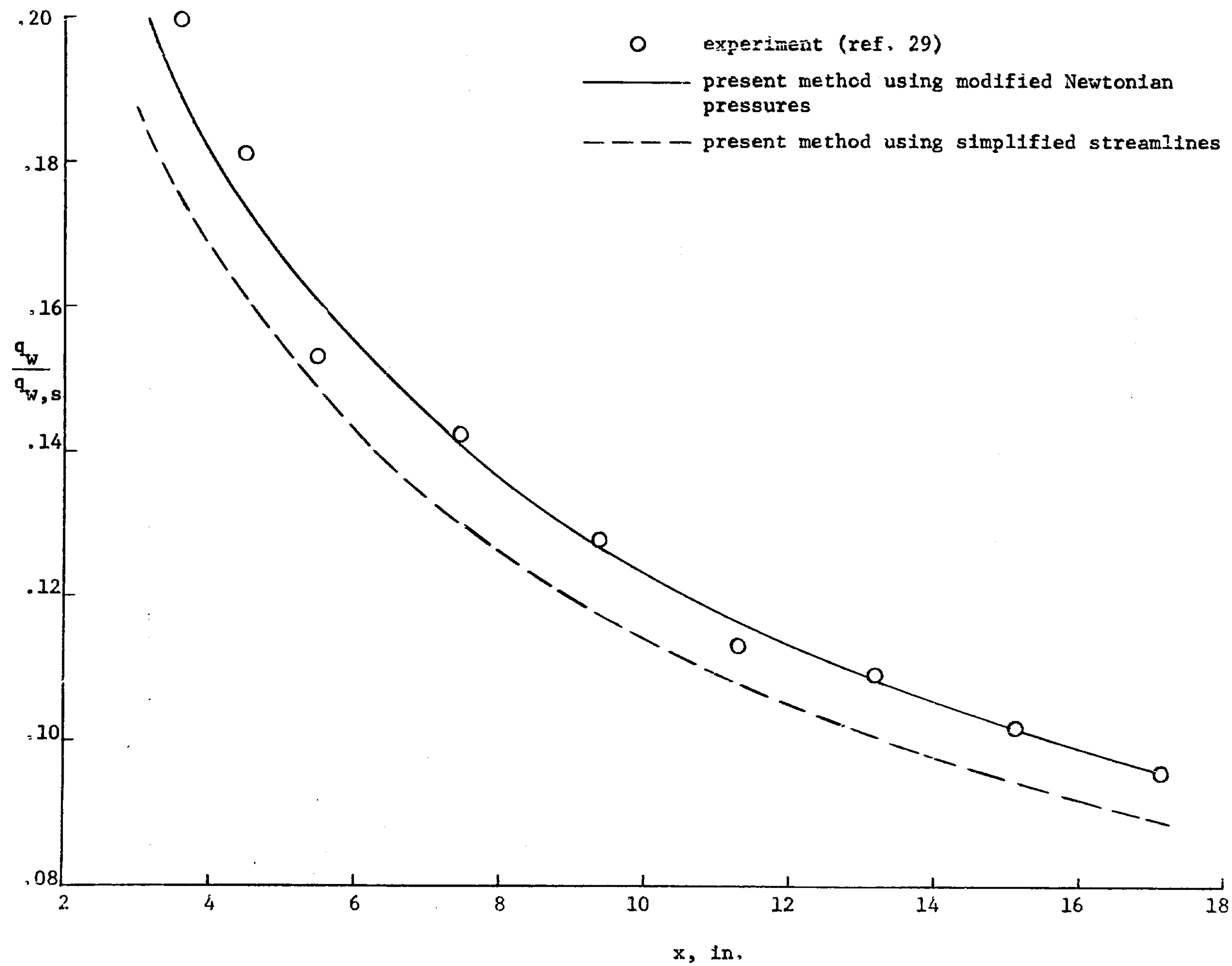

Figure 9. - Heating-rate ratio along windward streamline of a blunted 15° half-angle cone at $\alpha = 20°$, $M_\infty = 10.6$, $R_o = 0.375"$, and $p_s = 1.728 \times 10^5$ lb/ft^2.

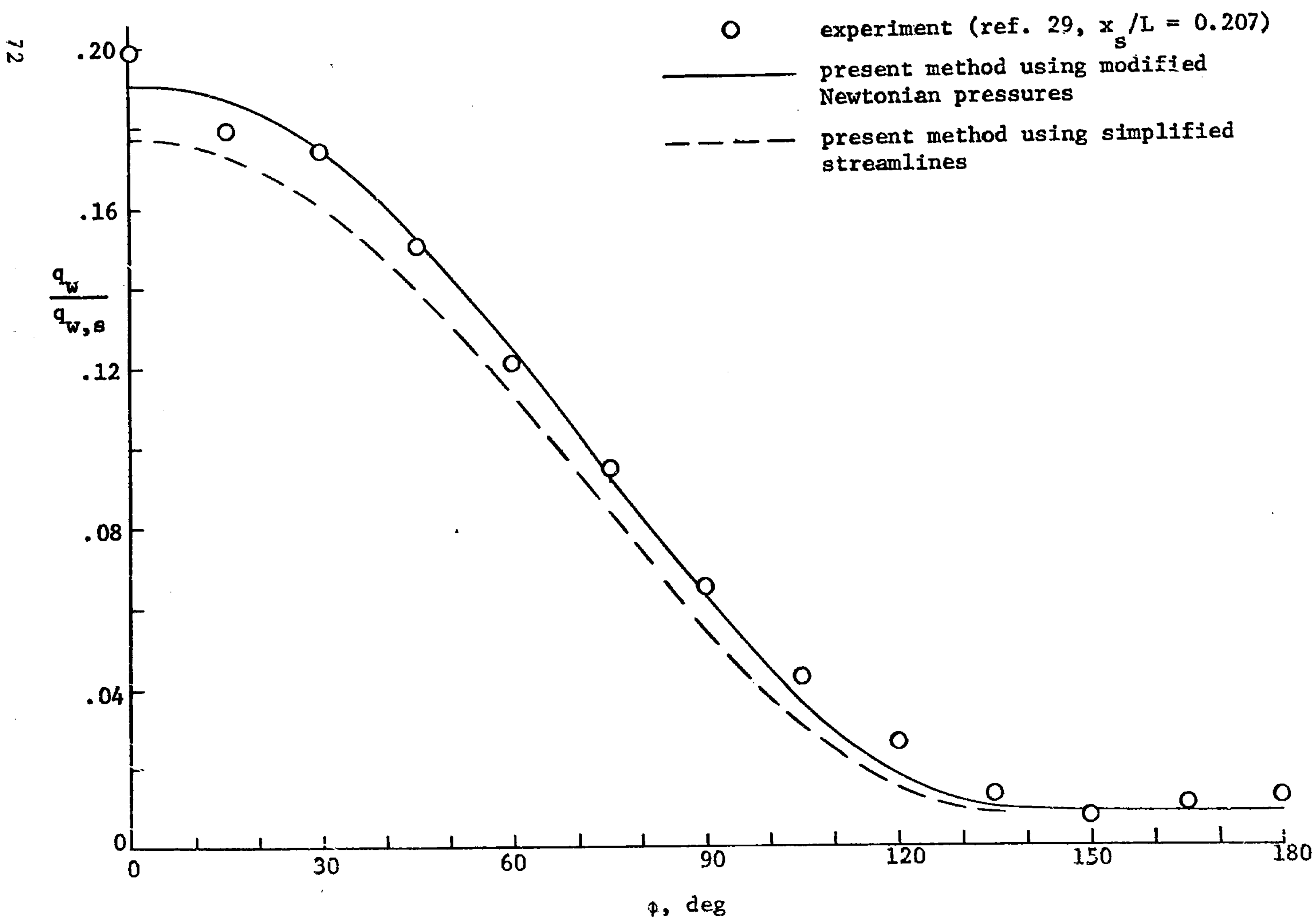

Figure 10. - Circumferential distribution of heating-rate ratio on a blunted 15° half-angle cone at $\alpha = 20°$, $M_\infty = 10.6$, $R_o = 0.375''$, $\rho_s = 1.728\times10^5$ lb/ft^2, and $x = 3.56''$.

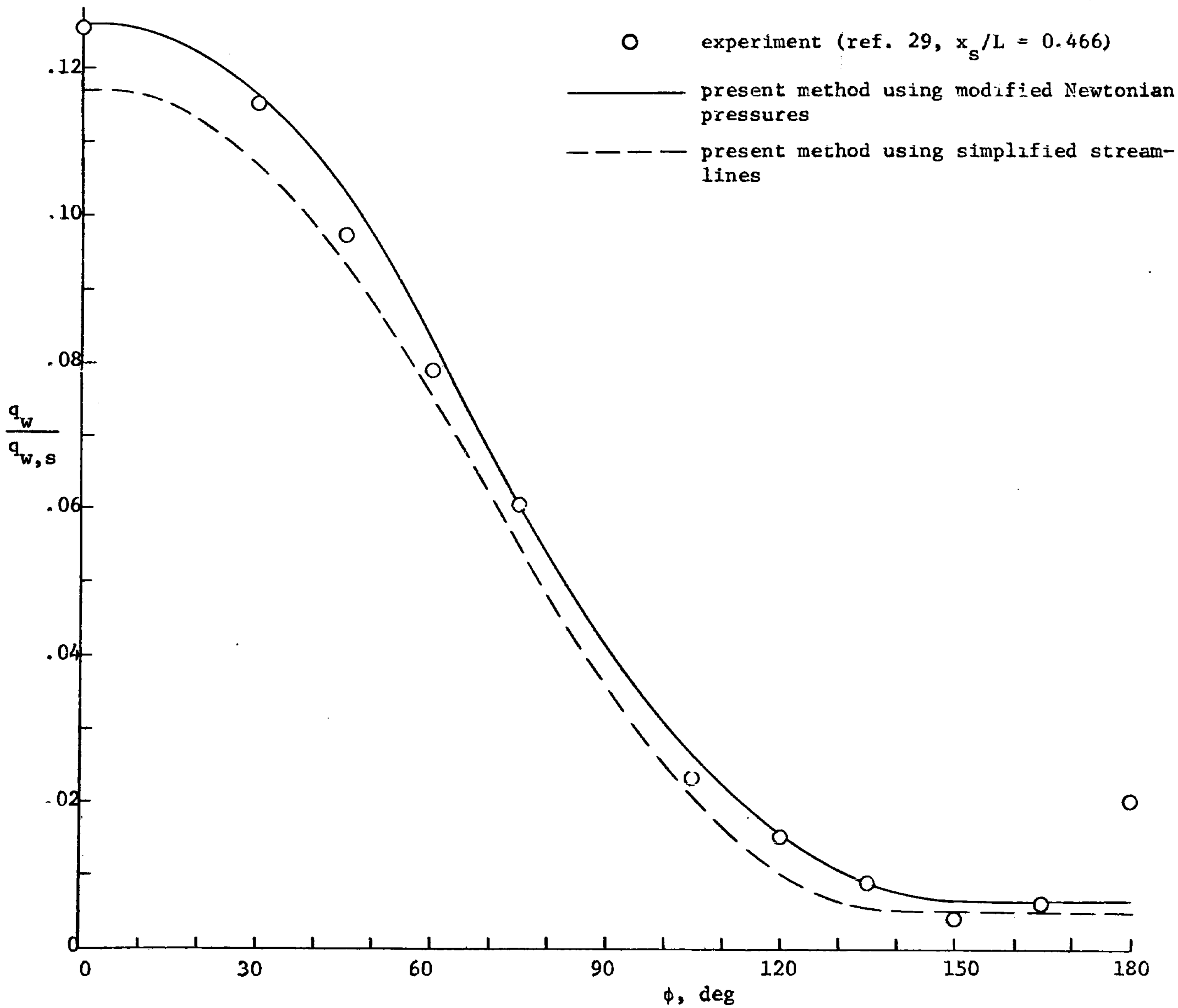

Figure 11. - Circumferential distribution of heating-rate ratio on a blunted 15° half-angle cone at α = 20°, M_∞ = 10.6, R_o = 0.375", p_s = 1.728x10^5 lb/ft^2, and x = 9.36".

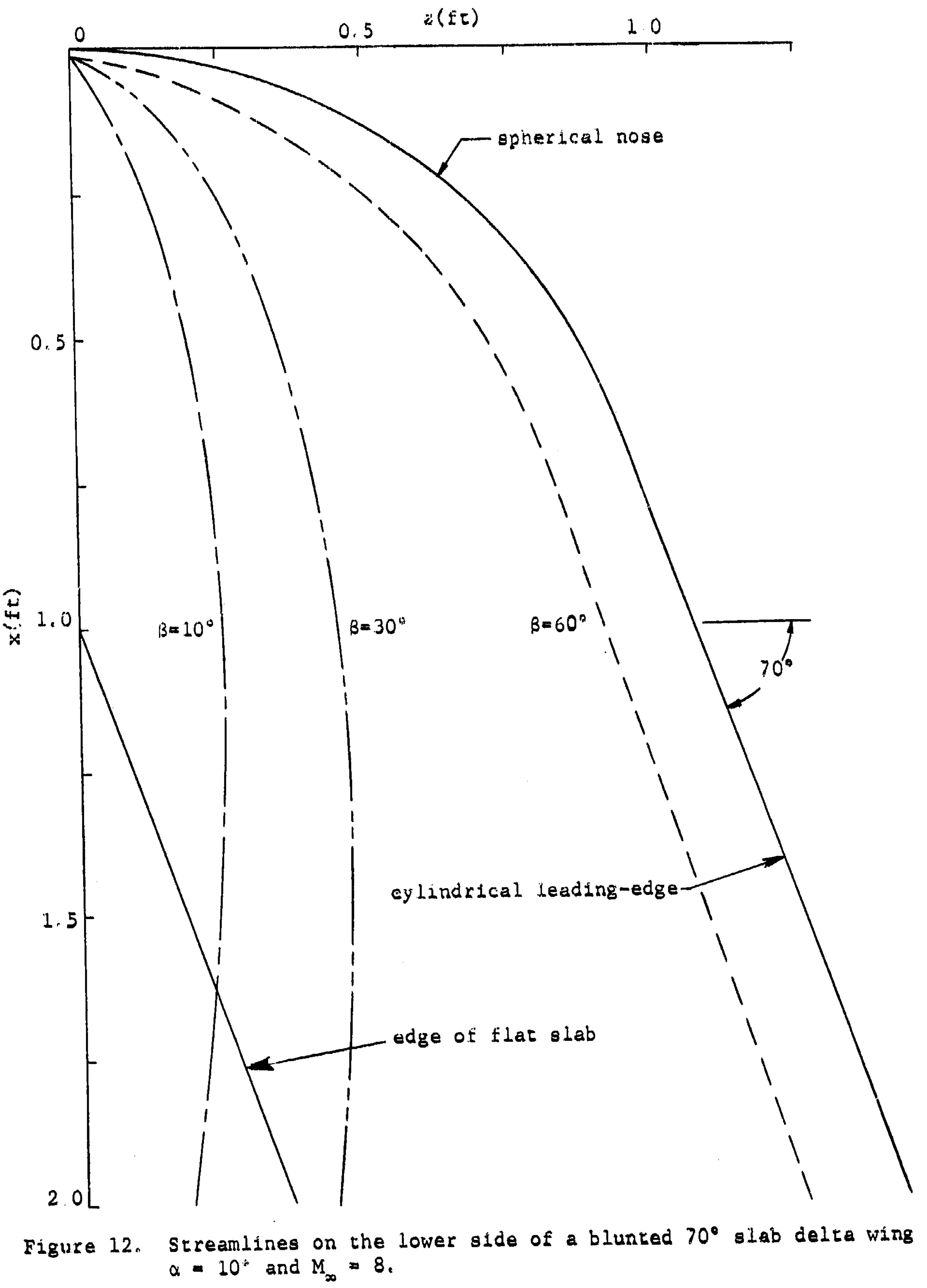

Figure 12. Streamlines on the lower side of a blunted 70° slab delta wing at $\alpha = 10°$ and $M_\infty = 8$.

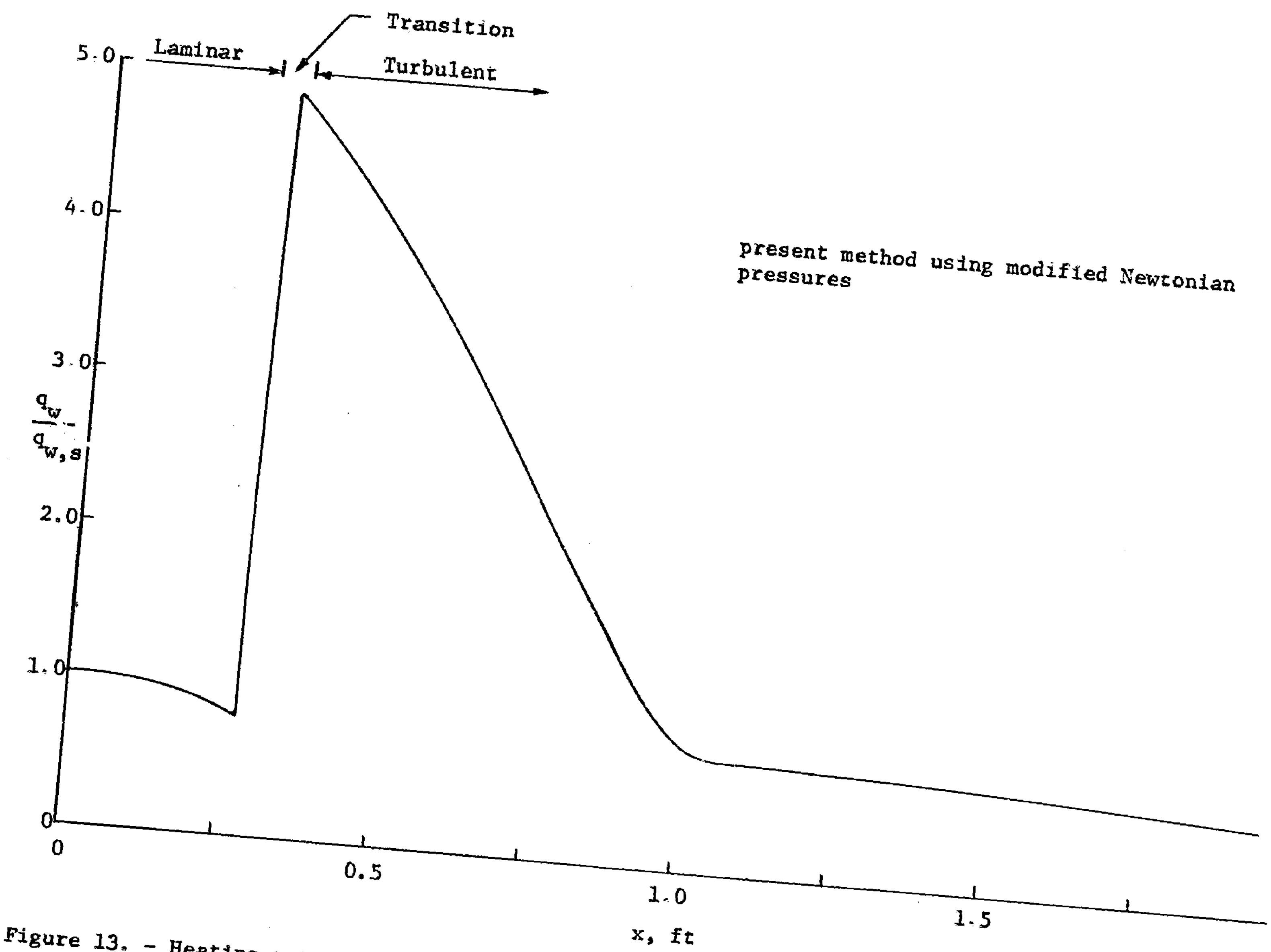

Figure 13. - Heating-rate ratio along windward streamline of a blunted 70° slab delta wing at $\alpha = 10°$ and $M_\infty = 8$.

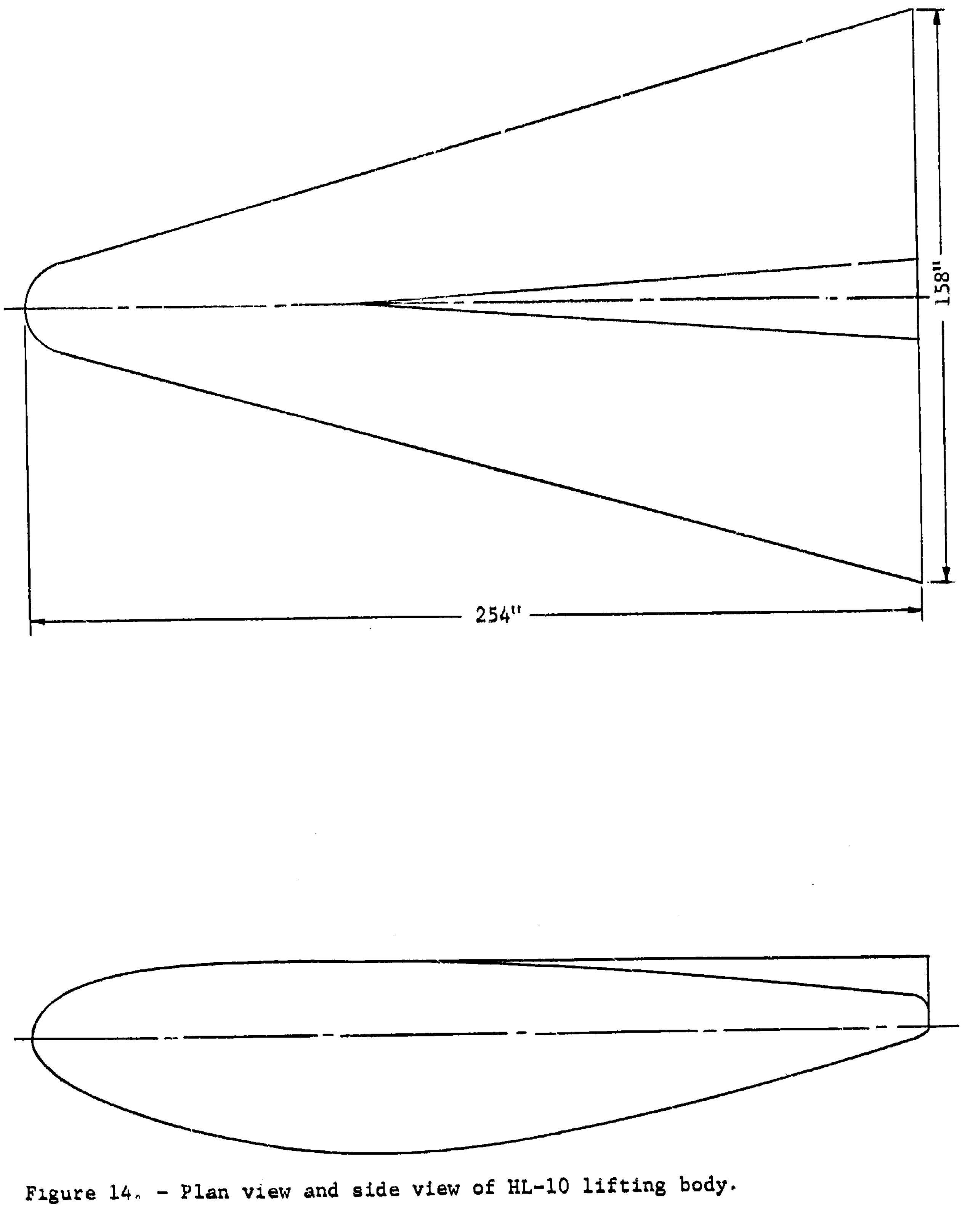

Figure 14. - Plan view and side view of HL-10 lifting body.

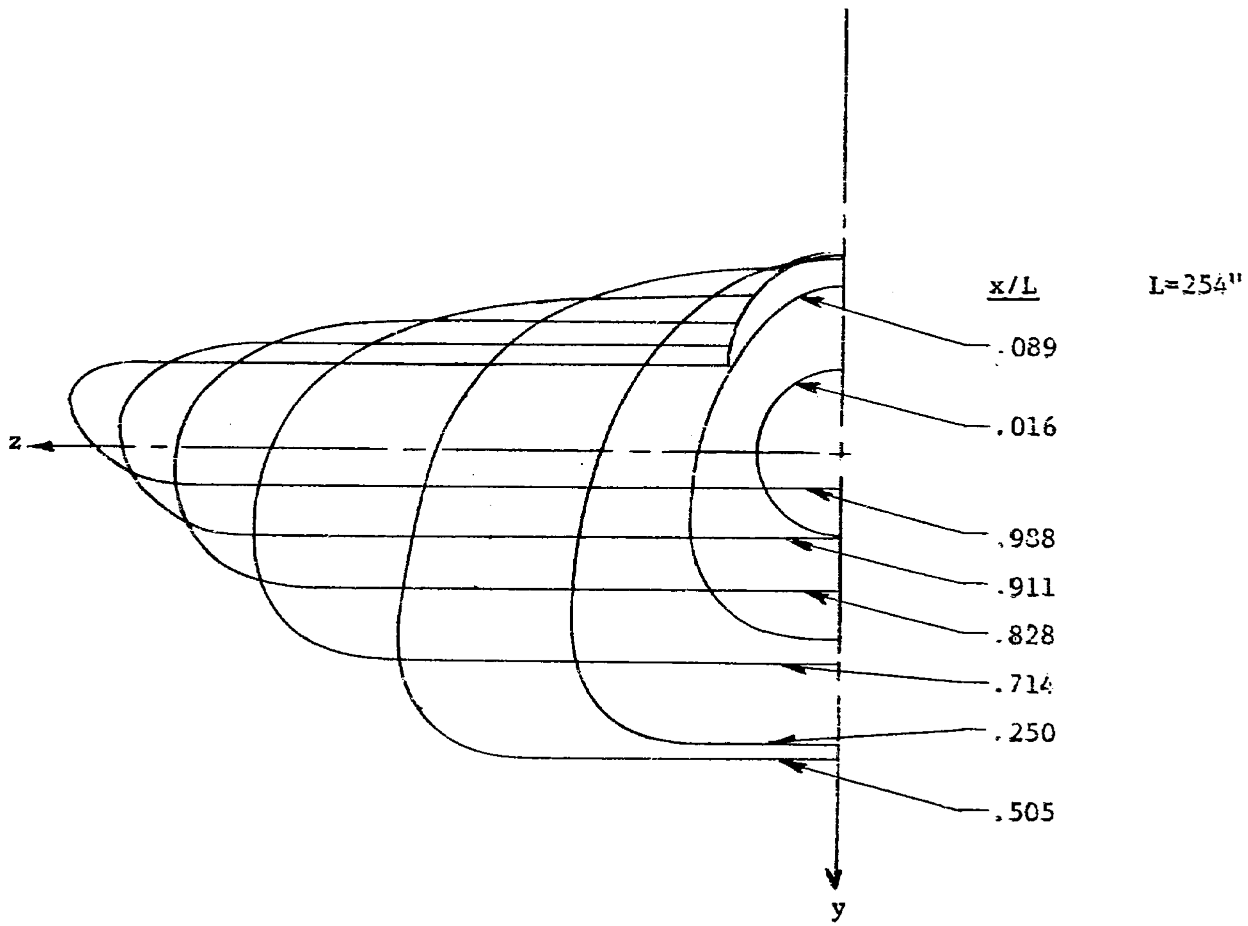

Figure 15. - Frontal cross sections of HL-10 lifting body.

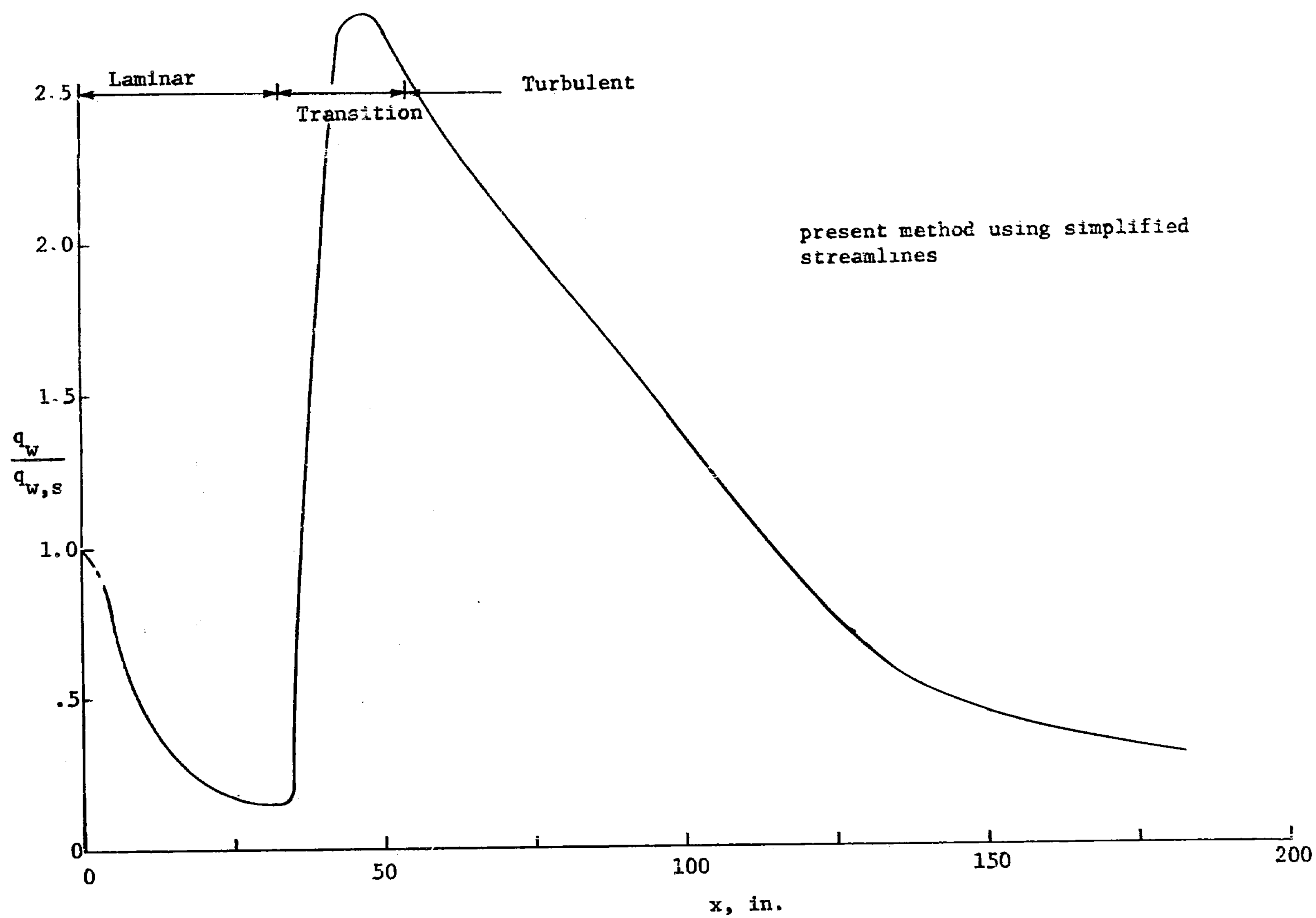

Figure 16. – Heating-rate ratio along windward streamline of HL-10 lifting body at $\alpha = 20°$ and $M_\infty = 10$.